Journal of Structural Geology 70 (2015) 95–118

Contents lists available at ScienceDirect

Journal of Structural Geology

journal homepage: www.elsevier.com/locate/jsg

Deformation within an exposed salt wall: Recumbent folding and extrusion of evaporites in the Dead Sea Basin

G.I. Alsop [a, *], R. Weinberger [b, c], T. Levi [b], S. Marco [d]

[a] Department of Geology and Petroleum Geology, School of Geosciences, University of Aberdeen, Aberdeen, UK
[b] Geological Survey of Israel, Jerusalem, Israel
[c] Department of Geological and Environmental Sciences, Ben Gurion University of the Negev, Beer Sheva, Israel
[d] Department of Geosciences, Tel Aviv University, Israel

ARTICLE INFO

Article history:
Received 22 October 2014
Received in revised form
19 November 2014
Accepted 25 November 2014
Available online 3 December 2014

Keywords:
Salt tectonics
Salt wall
Salt sheet
Sedom
Dead sea

ABSTRACT

Despite the enormous global interest in salt tectonics, which is largely driven by its importance to hydrocarbon exploration, direct field-based studies of salt exposed at the Earth's surface are rare. However, Mount Sedom, located at the western side of the Dead Sea Basin, presents one such opportunity for detailed analysis of salt and the associated sedimentary and structural record of its movement. The Sedom salt wall is a 10 km × 1.5 km N–S trending ridge comprising a range of Late Miocene-Pliocene evaporites and clastics, which have penetrated the overlying Pleistocene clastic sequence. The salt wall displays a moderate-steep west dipping western margin and an overturned (west-dipping) eastern flank. The sedimentary record of passive wall growth includes sedimentary breccia horizons that locally truncate underlying beds and are interpreted to reflect sediments having been shed off the crest of the growing salt wall. Structurally, the overturned eastern flank is marked by upturn within the overburden, extending for >300 m from the salt wall. Deformation within the evaporites is characterised by ductile folding and boudinage, while a 200 m thick clastic unit within the salt wall forms a tight recumbent fold traceable for 5 km along strike and associated with a 500 m wide inverted limb. This overturned gently-dipping limb is marked by NE-directed folding and thrusting, sedimentary injections, and a remarkable attenuation of the underlying salt from ~380 m to <20 m over just 200 m of strike length. The inverted limb is overlain by an undeformed anhydrite, gypsum and clastics caprock, thought to be the residue from a now dissolved salt sheet that extruded over the top of the fold. Expulsion of salt down the regional slope towards the NE, combined with subsequent dissolution of evaporites, may have resulted in local 'pinching shut' of the salt wall, leading to a distinctive hour-glass map pattern. This area also coincides with deposition of a thicker overlying clastic sequence, indicating continued subsidence of this part of the salt wall. Our detailed fieldwork forms the first direct observation and description of large recumbent folds within salt walls, and permits analysis below the limits of seismic resolution. It thereby allows more rigorous testing of salt tectonic models and mechanisms.

1. Introduction

Despite the enormous interest in salt tectonics that is largely driven by the importance attached to salt in hydrocarbon exploration (e.g. Archer et al., 2012), there are relatively few outcrop studies of salt diapirs, linear salt walls or allochthonous salt sheets. There are even fewer studies where we actually see halite exposed at the surface, reflecting the high solubility of salt and the extreme aridity necessary to preserve it at the Earth's surface. Outcrop studies of surficial salt flows in areas such as the Zagros of Iran enable examination of structures developed within salt glaciers (e.g. Talbot, 1979, 1998), while InSAR analysis allows precise rates of current salt extrusion to be determined (e.g. Weinberger et al., 2006b; Aftabi et al., 2010; Barnhart and Lohman, 2012). However, deformation in underlying units is largely hidden by the salt itself, although recently dissolved salt sheets in Yemen permit study of both salt vents and sediments inferred to underlie the former salt sheet (e.g. Davison et al., 1996). In other areas, salt is suggested to

* Corresponding author.
E-mail address: Ian.Alsop@abdn.ac.uk (G.I. Alsop).

http://dx.doi.org/10.1016/j.jsg.2014.11.006
0191-8141/

have created surficial flows, but these are either not preserved at outcrop (e.g. Masrouhi and Koyi, 2012; Ringenbach et al., 2013; Masrouhi et al., 2014), or have been heavily overprinted by contraction in settings such as La Popa in Mexico (Giles and Rowan, 2012; Rowan et al., 2012), or even more extreme orogenesis in the Alps (e.g. Graham et al., 2012). Although salt may not actually be exposed at outcrop, a number of studies have recently been undertaken into fault and fracture patterns within overburden adjacent to buried or removed salt diapirs (e.g. Quintà et al., 2012; Poprawski et al., 2014) and salt walls (e.g. Storti et al., 2011).

This general lack of outcrop work on salt means that analysis of salt diapirs and salt walls has been forced to rely heavily on analogue modelling using polymers with a variety of sand (e.g. Hudec and Jackson, 2011; Dooley et al., 2014) and glass bead materials (e.g. Alsop, 1996), numerical modelling (e.g. Albertz and Ings, 2012; Fuchs et al., 2014), combined with seismic analysis of salt sheets (e.g. Quirk and Pilcher, 2012; Jackson et al., 2014). In addition, the mechanical significance of multilayer evaporites where anhydrite, halite and clastics are interlayered on a variety of scales resulting in potential strain partitioning within salt sheets and diapirs (e.g. Talbot and Jackson, 1987), is receiving increased attention due to improved seismic analysis in areas such as the eastern Mediterranean (e.g. Cartwright et al., 2012), offshore Brazil (e.g. Fiduk and Rowan, 2012) or North Sea (e.g. Strozyk et al., 2012). However, once again there are relatively few outcrop studies of deformation within a range of evaporite and clastic lithologies forming salt walls, although some have been undertaken in Canada (e.g. Alsop et al., 2000; Vargas-Meleza et al., 2015; Harrison and Jackson, 2013), Turkey (e.g. Ringenbach et al., 2013) and Morocco (e.g. Saura et al., 2014).

The Dead Sea Basin which receives <50 mm precipitation per year is one area where halite together with other evaporites are exposed at the surface, thereby permitting detailed structural and stratigraphic relationships to be directly observed (Fig. 1a, b). It therefore represents a crucial 'testing ground' of ideas and concepts largely developed through seismic interpretation and/or modelling studies. The extreme aridity also results in superb levels of exposure, whilst continuing uplift of Mount Sedom leads to deep erosional incision and exposure of the surrounding overburden. This overburden is a mixed sequence of clastics and marls that have been recently dated and allow detailed preservation of salt-influenced sedimentary and tectonic structures. In addition, the regional tectonic framework within the strike-slip dominated Dead Sea Fault system is well understood (e.g. Garfunkel, 1981; Joffe and Garfunkel, 1987), allowing pristine relationships to be preserved without the complication of a contractional overprint (Fig. 1a, b). The salt is relatively young (Late Miocene-Pliocene), and continues to move today allowing a greater appreciation of the factors that influence salt tectonics. This study builds on a substantial database of pre-existing work including detailed geological mapping at 1:10,000 scale (Zak, 1967; Agnon et al., 2006), isotopic dating (e.g. Torfstein et al., 2009; Matmon et al., 2014), records of Holocene uplift within cave systems in the salt (e.g. Frumkin, 1996a, b, c), together with InSAR analysis of current salt movement (Weinberger et al., 2006a, b).

In this case study, we use the Sedom salt wall to address a number of major questions relating to the general geometry and kinematics of salt walls and their associated extrusive salt sheets including:

a) How are large recumbent folds created within a salt wall?
b) What are the kinematics and mechanics of recumbent folds within a salt wall?
c) Why are outward-verging folds created on the flank of a salt wall?

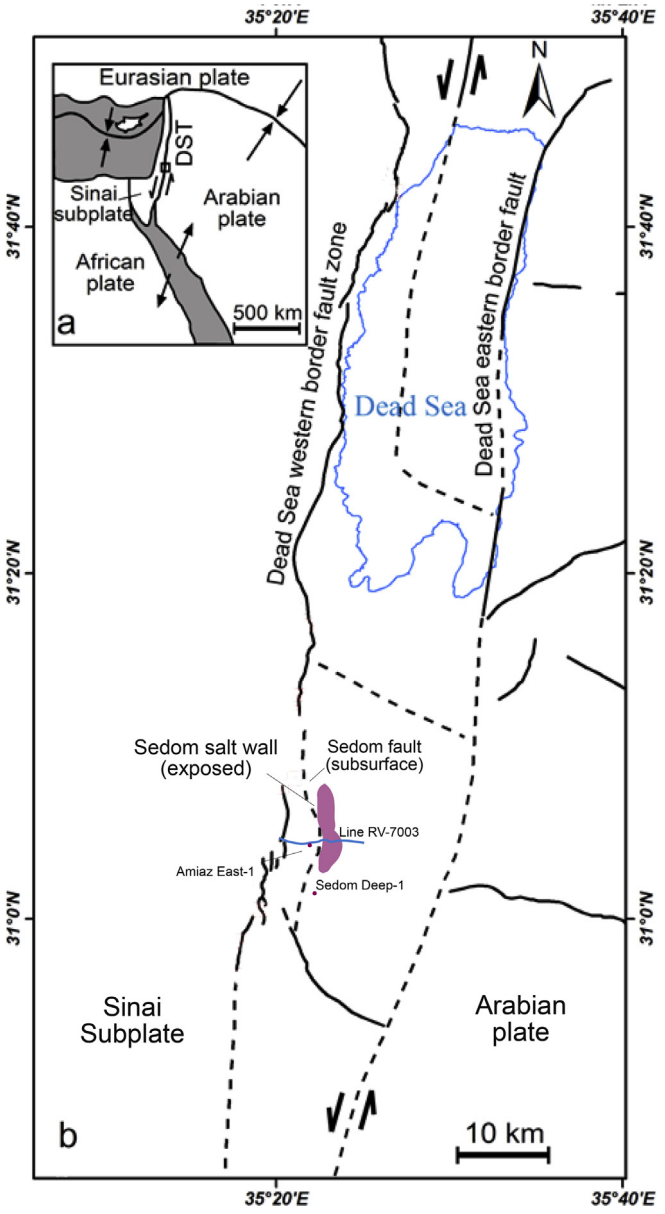

Fig. 1. a) Tectonic plates in the Middle East. General tectonic map showing the location of the present Dead Sea Fault (DSF). The Dead Sea Fault is a left-lateral fault that transfers the opening motion in the Red Sea to the Taurus – Zagros collision zone with the Eurasian plate. Location of b) shown by the small box on the DSF. b) Map of the Dead Sea showing the position of the exposed Sedom salt wall and strands of the Dead Sea Fault (based on Sneh and Weinberger, 2014). The locations of the RV-7003 seismic line, together with the Sedom Deep-1 and Amiaz East-1 boreholes are shown, as is the subsurface trace of the Sedom Fault.

d) How is overturned salt dramatically thinned on the flank of a salt wall?
e) What creates the pinched 'hour-glass' shape of a salt wall?

The scientific motivation behind our field-based approach is thus to provide a better understanding of the detailed stratigraphic and structural relationships within and around salt walls that would normally be lost as they are below the limits of seismic resolution. In detail, this includes: a) a greater understanding of the role that recumbent fold limbs play in the lateral extrusion of salt, and: b) the nature of deformation in multilayer evaporite (rather than just halite-dominated) salt walls. This ultimately allows us to

more rigorously test salt tectonic models with obvious implications for hydrocarbon exploration.

2. Regional overview of stratigraphy and basin evolution

The Sedom salt wall is a ~10 km long N–S trending ridge that rises ~240 m above the level of the Dead Sea (Fig. 1a, b). Seismic profiles across the Sedom salt wall suggest that it is located adjacent to the underlying Sedom Fault, a major ~N–S trending extensional fault that may have focussed the upward flow of salt from depths of 3–4 km (Gardosh et al., 1997; Weinberger et al., 2006a) (Fig. 1b and Fig. 2). The wall is commonly divided into northern and southern segments each of which is ~4 km long and ~1.5–2 km wide at surface (Fig. 3). These two segments are separated from one another by a 2 km long central 'pinched' section (or 'neck') where the margins of the wall converge and its width reduces to just 800 m. This gives the Sedom wall a distinctive hourglass shape in map view (Fig. 3). The western margin of the Sedom wall dips moderately to steeply towards the west, while the eastern flank also dips variably towards the west and is overturned. The northern limit of the Sedom salt wall is marked by moderate dips towards the north, where the 'nose' of the salt wall plunges below the surrounding overburden (Fig. 3).

The Sedom salt wall is formed of the Sedom Formation predominantly comprising evaporites (75%) including halite, anhydrite and thin dolomites, interbedded with thinner clastics formed of siltstone, mudstone, clay and sandstones (Zak, 1967; Frumkin, 2009). The Sedom Formation is subdivided into five members (Table 1; Zak, 1967). In detail, the evaporite sequence comprises the stratigraphically lowermost Karbolet Salt and Shale Member that is followed by the Lot Salt Member (Table 1). This is separated from the younger Mearat Sedom Salt Member by the intervening (up to 200 m thick) Bnot Lot Shales Member dated at 6.2 and 5.0 ± 0.5 Ma (^{10}Be and terrestrial cosmogenic nuclide (TCN) ages from Matmon et al., 2014) (Table 1).

This Late Miocene-Pliocene evaporite sequence penetrates the surrounding Pleistocene Amora and Lisan formations, that form the overburden to the salt wall, via marginal faults and shear zones (Zak and Freund, 1980, Fig. 3).The Amora Formation is subdivided into three members (Agnon et al., 2006, Table 1). The Lower Amora Member comprises 200 m of shales, sandstones and conglomerates and forms the lowest stratigraphic level exposed at outcrop dated at 740 ± 66 ka (U series ages from Torfstein et al., 2009). This is overlain by the Amora Salt Member which is a 10 m thick halite interval estimated via U–Th at 420 ± 10 ka (Torfstein et al., 2009). Finally, the 195 m thick Upper Amora Member comprising shales, sandstones and conglomerates sits stratigraphically above the salt member, and has been dated at the Peratzim 2 borehole site (immediately west of Mount Sedom) as ranging between 340 and 80 ka (Torfstein et al., 2009).

Although only 400–450 m of Amora Formation are actually exposed next to the Sedom salt wall, the overall Plio-Pleistocene sediment (overburden) attains thicknesses of 5500 m in the southern Dead Sea Basin (Al-Zoubi and ten Brink, 2001; Weinberger et al., 2006a). Immediately to the SE of Sedom, the Sedom Deep-1 drill hole penetrated a 3700 m thick fluvio-lacustrine series which overlies a 900 m thick evaporite series (Fig. 1b and Fig. 2). To the west of Mount Sedom, the Ami'az East-1 drill hole penetrated a 1300 m thick evaporite series overlain by 1900 m thick fluvio-lacustrine series (Weinberger et al., 2006a) (Fig. 1b and Fig. 2). The base of the Lower Amora Member within this borehole has been recently dated as 3.3 ± 0.9 Ma, while approximately 500 m stratigraphically higher, the Lower Amora sediments are dated as 2.7 ± 0.7 Ma (Matmon et al., 2014). Overall, the Sedom Formation thickens towards the depocentre and thins towards the western margin of the basin (e.g. Zak, 1967) (Fig. 2). Salt flowing into the Sedom salt wall is considered to have been largely sourced from the east due to differential overburden loading, with only a minor component derived from the west (Weinberger et al., 2006a). There is therefore no correlation in

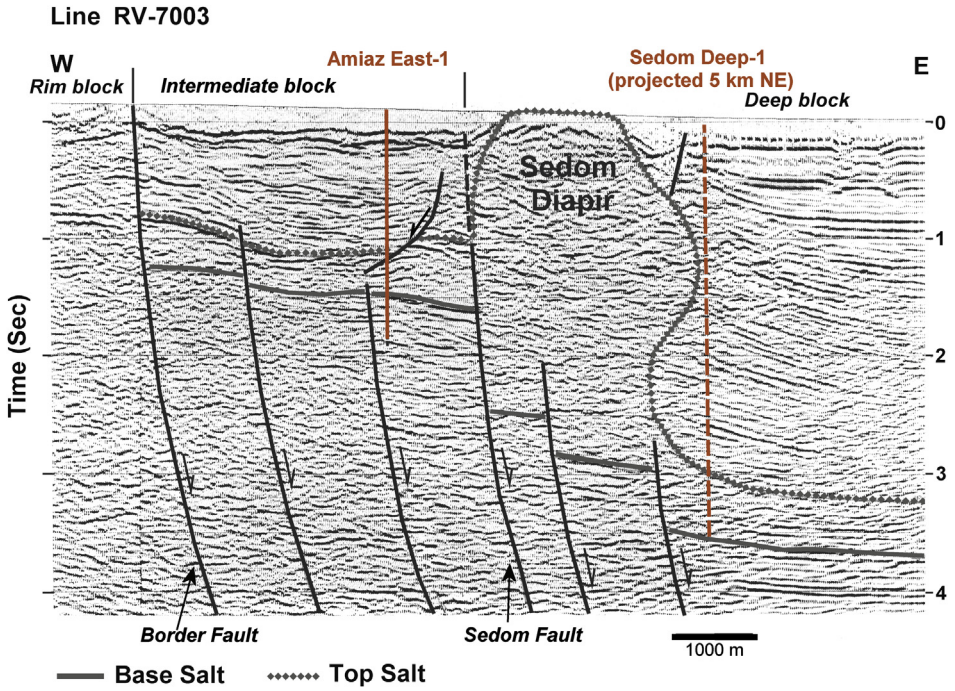

Fig. 2. Time migrated interpreted seismic profile RV-7003 across the Sedom salt diapir and adjacent overburden sediments (from Weinberger et al., 2006a). The seismic highlights the position of the sub-surface Sedom Fault, that is considered to have controlled the location of the Sedom salt wall, and divides the Dead Sea Basin into intermediate and deep blocks. The underlying source layer of salt (Sedom Fm.) is traced across the Sedom Fault, where it drops down into the deep block marked by much greater overburden thicknesses. The locations of the RV-7003 seismic line, together with the Sedom Deep-1 and Amiaz East-1 boreholes that constrain overburden thicknesses are shown in Fig. 1b.

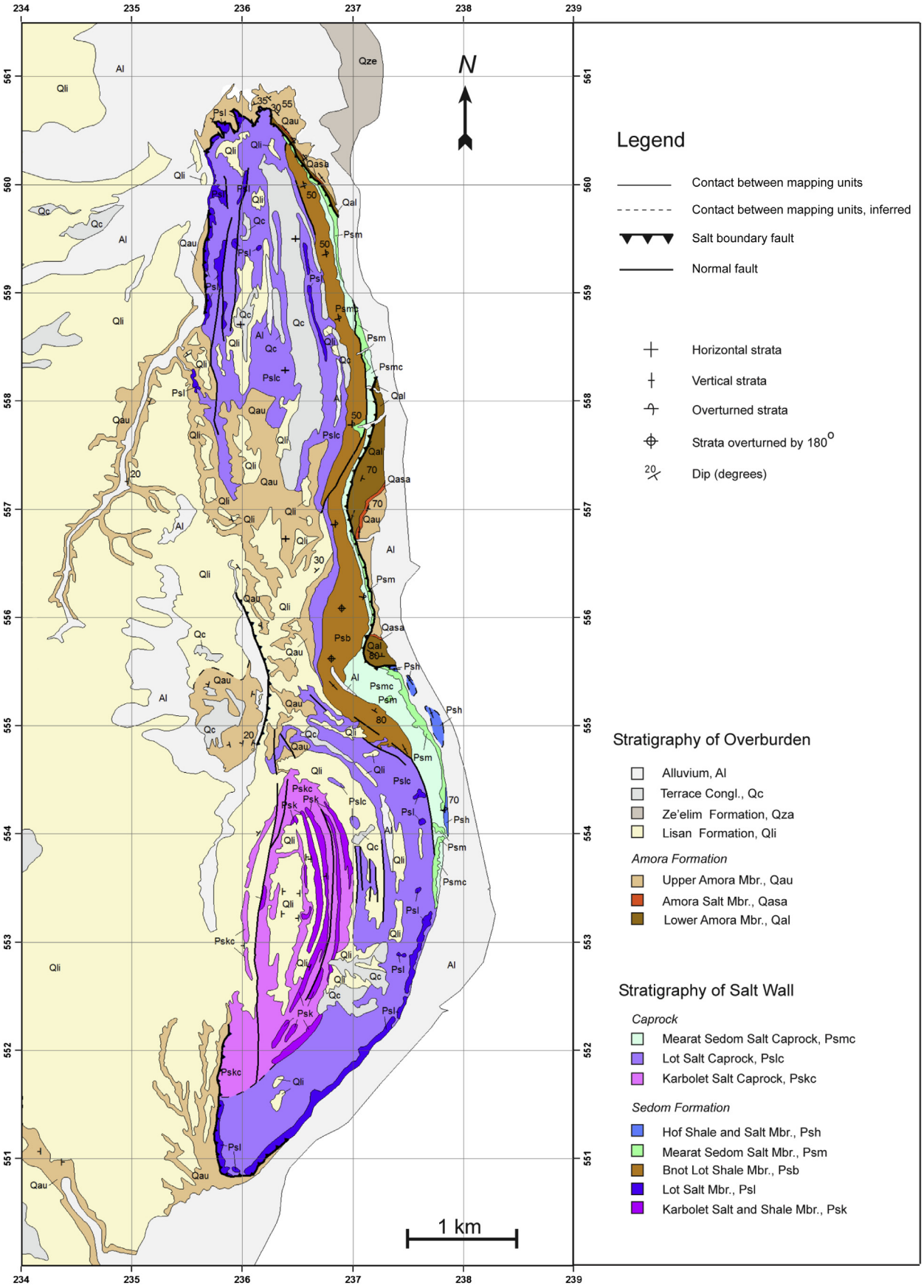

Fig. 3. Geological map of the Sedom salt wall and its vicinity based on Zak (1967) and Agnon et al. (2006). The area of interest in this study is north of the central 'pinched' segment and in particular the eastern flank of the Sedom salt wall (north of Grid 555). See Fig. 1b for location.

Table 1
Generalised stratigraphy and ages of the Sedom Formation that comprises the Sedom salt wall, and the Amora and Lisan Formations that form the overburden to the salt. Note that dissolution of salt members leads to local caprocks being preserved at the surface. TCN – Terrestrial cosmogenic nuclide burial ages.

Formation	Member	Description and age
Lisan Formation		40 m of aragonite-rich lacustrine sediments dated between ~70 ka and 14 ka (U-series and ^{14}C, Haase-Schramm et al., 2004).
Amora Formation (overburden to Sedom salt wall)	Upper Amora Member	200 m of fluvio-lacustrine shales, sandstones and conglomerates ranging in age between 340 and 80 ka (Torfstein et al., 2009).
	Amora Salt Member	10 m thick halite unit dated at 420 ± 10 ka (U–Th ages from Torfstein et al., 2009)
	Lower Amora Member	200 m of fluvio-lacustrine shales, sandstones and conglomerates exposed at outcrop. Dated at 740 ± 66 ka (U series ages from Torfstein et al., 2009).
Sedom Formation (forms the Sedom salt wall)	Hof Shale and Salt Member	Up to 90 m of halite and shales (Zak et al., 1968)
	Mearat Sedom Salt Member	Up to 250 m of halite, anhydrite and minor clastics
	Bnot Lot Shales Member	Up to 200 m thick sandstones and shales dated at 6.2 and 5.0 ± 0.5 Ma (^{10}Be TCN burial ages from Matmon et al., 2014)
	Lot Salt Member	Up to 800 m of halite, anhydrite and minor clastics
	Karbolet Salt and Shale Member	550 m minimum thickness of halite and shale units (base not observed and not dated).

evaporite stratigraphy from the west to east flank of the salt wall, with the 'suture' separating the two evaporite sources considered to lie to the west of the Bnot Lot Shales Member in the northern part of Mount Sedom (Frumkin, 1996c; Weinberger et al., 1997, 2006a) (Fig. 3).

The crest of the Sedom salt wall is covered by a 40 m thick insoluble caprock, which consists mainly of anhydrite, gypsum, as well as minor marl, clay, dolomite and sandstone fragments. The caprock is considered to have formed during dissolution of the various salt members (Zak and Freund, 1980). Zak and Freund (1980, p. 568) note that the Sedom Formation contains 5% (by weight) insoluble residue and suggest that 40 m of caprock therefore required the dissolution of 600–800 m of salt. In general, caprocks are considered to thicken by 'underplating' as

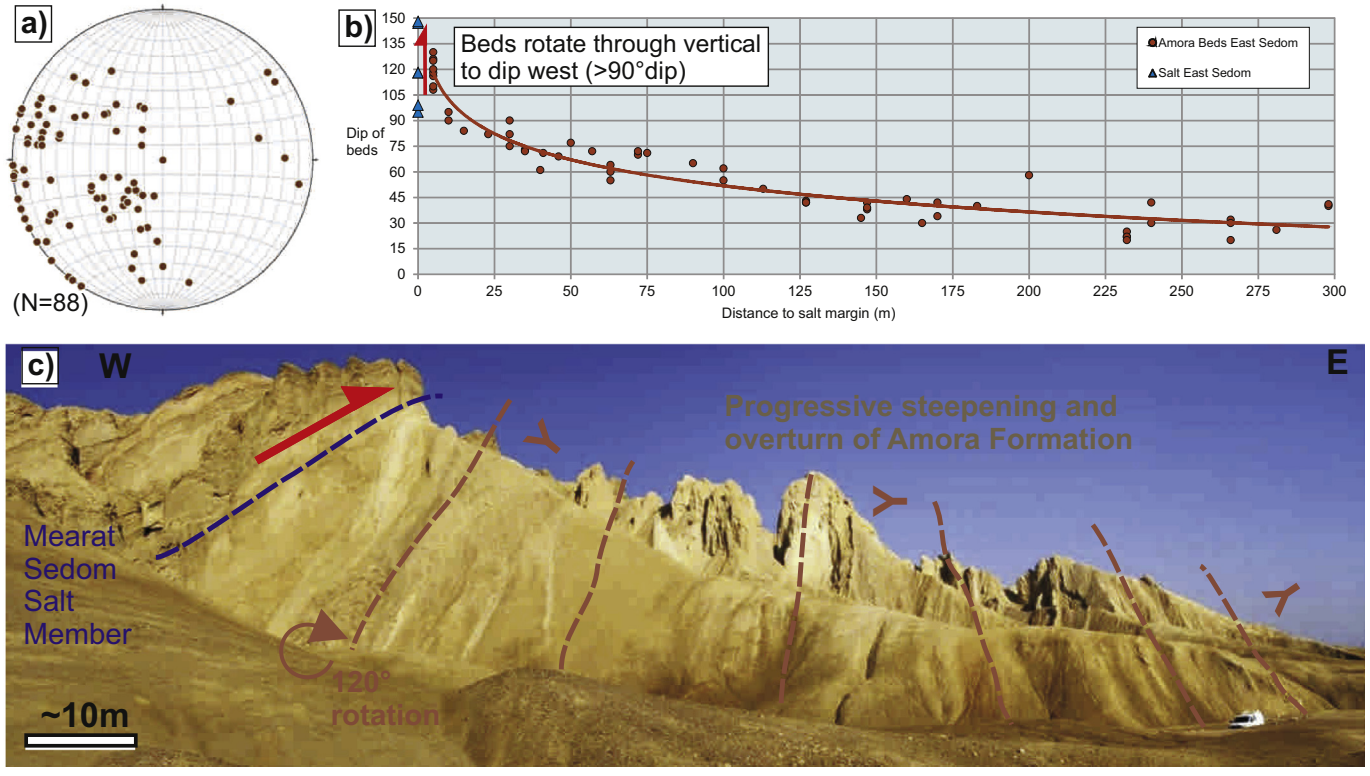

Fig. 4. a) Stereonet of poles to bedding ($N = 88$) collected from the Amora Fm. that forms the overburden along the eastern margin of the Sedom salt wall. b) Graph and best–fit curve of distance from the eastern margin of the Sedom salt wall compared to angle of bedding dip within the Amora Fm ($N = 63$). Where easterly-dipping beds have rotated through the vertical to become inverted and westerly-dipping, they are shown as dipping at angles >90°. c) Photograph of upturned Amora Fm. adjacent to the eastern margin of the salt wall (N31.09965°; E35.38986°). The inferred direction of younging is shown by the 'Y' symbol. The Mearat Sedom Salt Member is now structurally above the overburden comprising the Amora Fm.

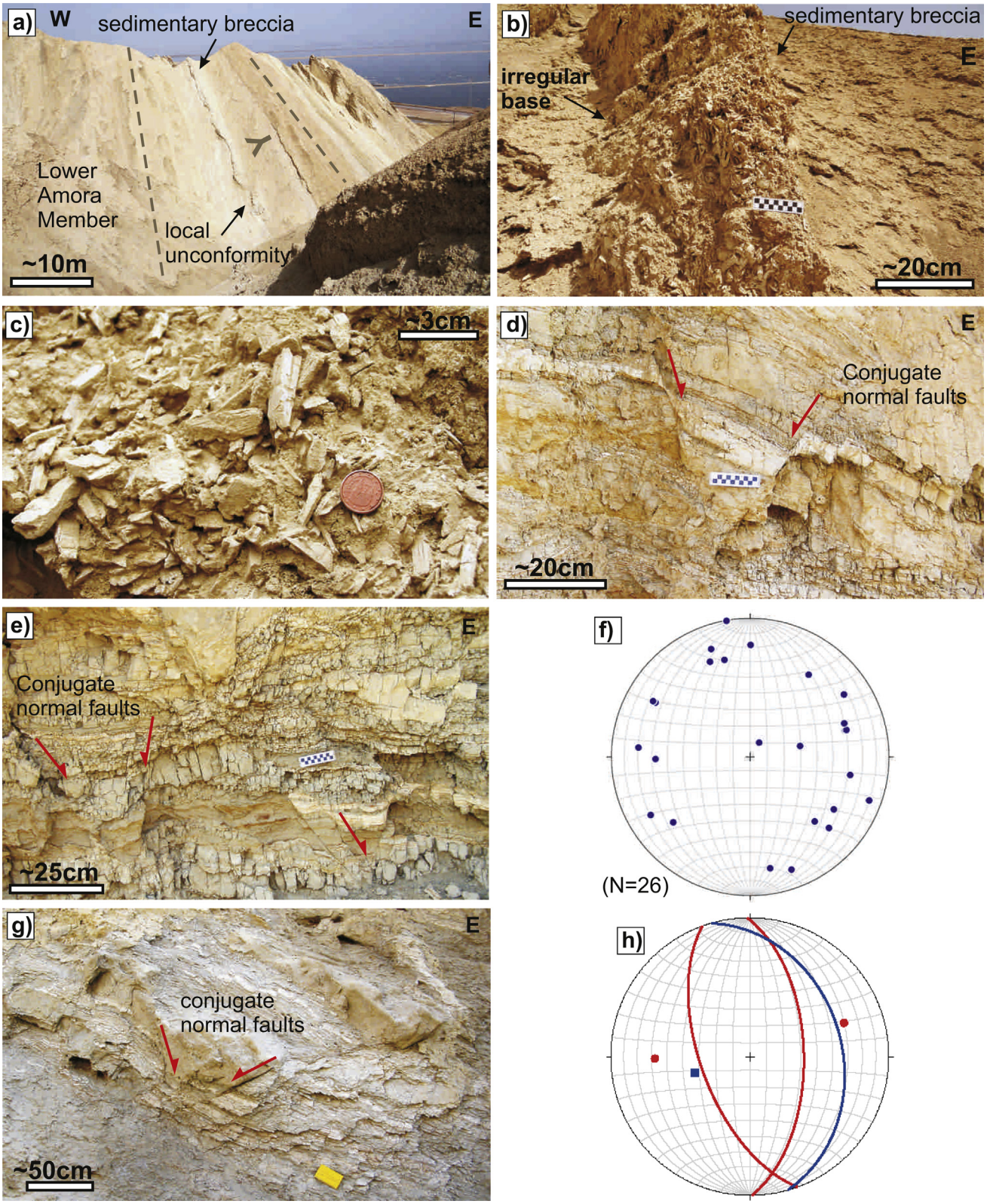

Fig. 5. Photographs of the Lower Amora Member that forms overburden to the eastern margin of the Sedom salt wall. The inferred direction of correct way up younging is shown by the 'Y' symbol. The Lower Amora Member contains a sedimentary breccia that displays a) a local angular unconformity with underlying beds (shown by dashed line) (N31.099655°; E35.389623°), b) an irregular erosive base (N31.099655°; E35.389623°), and c) angular sandstone and shale fragments up to 4 cm long (N31.099655°; E35.389623°). d), e) Conjugate extensional fractures within gently east-dipping beds of the Lower Amora Member from the eastern margin of the Sedom salt wall (N31.137103°; E35.381932°). f) Stereonet of poles to fractures ($N = 26$) from the Amora Fm. on the eastern margin of the Sedom salt wall. g) Photograph of conjugate extensional fractures within the Lower Amora Member (N31.137103°; E35.381932°), together with associated stereonet (h) showing fractures (red great circles and poles) and gently east-dipping bedding (blue great circle and pole). Scales are provided by a 15 mm diameter coin, a 10 cm long chequered rule and a 20 cm long yellow notebook. (For interpretation of the references to colour in this figure legend, the reader is referred to the web version of this article.)

more salt is dissolved from below. The gentle deflection of clastic marker layers as they pass from the Mearat Sedom Salt Member (Table 1) into the overlying caprock reflects this dissolution and collapse of salt to create the caprock (Zak, 1967). The caprock above the Mearat Sedom Salt Member and Lot Salt Member has been generated during dissolution ranging from pre-Upper Amora (340–80 ka) (Zak and Freund, 1980), to pre-Lisan Formation.

The Pleistocene Lisan Formation overlies the Amora Formation and caprock, and consists of up to 40 m of aragonite-rich and detrital-rich laminae forming a varved lacustrine sequence, dated between ~70 ka and 14 ka by U-series and ^{14}C (Haase-Schramm et al., 2004; references therein, Table 1). The base of the Lisan Formation locally sitting on top of the Sedom salt wall has been dated as 43 ka, and has been carried up to 100 m above the regional elevation (Weinberger et al., 2007). The age of the top of the Lisan Formation on Mount Sedom is 15.5 ka, and it has been uplifted by 75 m since then at an average uplift rate of ~5 mm/year (see detailed calculations in Weinberger et al. (2007)). InSAR analysis reveals current uplift rates in the order of 5.5–8 mm/year (Weinberger et al., 2006b).

3. Structural record of salt movement from within the overburden to the salt wall

This study focuses on the central and northern parts of the Sedom salt wall, and in particular its eastern margin that dips variably towards the west and is significantly overturned.

3.1. Rotation and upturn of beds towards the salt margin

The eastern margin of the Sedom salt wall is marked by a progressive and sequential upturn of bedding within the Amora Formation that forms the overburden to the salt. Bedding typically dips at variable angles towards the east, with some overturned bedding dipping gently towards the west (Fig. 4a). The overall profile displays a steady increase in easterly-directed dips from ~30° at 300 m from the salt wall (beyond which the Amora Formation is covered by recent deposits and the Dead Sea) to ~50° at 100 m (Fig. 4b, c). The dips then rapidly increase with the inner-most 50 m of overburden adjacent to the salt being marked by an almost exponential increase in dips, where bedding has been rotated into subparallelism with the steep margin of the salt wall (Fig. 4b, c). The eastern flank of the central and northern segments of the salt wall displays a complete overturning, so that it now dips moderately west. In this situation, the 'overburden' then sits structurally below the salt and is inverted (Fig. 4c).

3.2. Local sedimentary breccias

On the eastern flank of the Sedom salt wall, local sedimentary breccia layers form part of bedded shales and sands exposed in the Lower Amora Member. These horizons are 1–1.5 m thick, display irregular bases and locally define a small angular unconformity with the underlying Amora sequence (Fig. 5a). They contain 1–2 cm long angular shale fragments that locally are up to tens of cm, and are graded indicating younging towards the east (Fig. 5b, c). This deposit is considered very proximal to its source as friable shale fragments will not transport far without breaking up. The most likely scenario is that the Lower Amora Member was over steepened during rotation of bedding noted above, and shales were consequently shed off the crestal area of the growing Sedom salt wall. These observations collectively suggest that the Sedom salt wall already had bathymetric expression during deposition of the Lower Amora Member.

3.3. Extensional faulting

Conjugate normal fault systems are developed throughout the Amora Formation adjacent to the eastern margin of the Sedom salt wall (Fig. 5d, e). These fractures and faults are moderately to steeply dipping and display variable trends (Fig. 5f). They typically exhibit cm-scale extensional displacements, and maintain high angles to rotated bedding (Fig. 5g, h). This suggests that they formed relatively early and are considered to relate to stretching of beds as they accommodated upward diapiric movement.

4. Structural record of salt movement from within the salt wall

4.1. Minor NE-verging folds and thrusts within evaporites and shales of the salt wall

Tight to isoclinal, NE-verging metre scale folds displaying type 2 similar geometries (Ramsay, 1967) are developed within halite-rich units of the Mearat Sedom Salt Member along the NE margin of the Sedom salt wall (Fig. 6a,c,e,f,g). These gently plunging, NNW-SSE trending folds deform the gentle-moderate SW-dipping bedding within the salt, and are associated with moderate-steep SW-dipping axial planes (Fig. 6a–d). Some tight NE-verging folds have had their upper limbs (Fig. 6a,c) or lower limbs (Fig. 6e) attenuated and replaced by NE-directed thrusts, while other NE-verging folds were truncated by an overlying dissolution surface termed the 'salt mirror' (Fig. 6f) (Farkash et al., 1951; Zak, 1967; Zak and Freund, 1980).

The Bnot Lot shales Member overlying the Mearat Sedom Salt Member also contains NE-verging folds, and has been thrust towards the NE (Fig. 7a–d). The Bnot Lot shales Member is also marked by locally west-verging 'backfolds' associated with intense fracturing (Fig. 7c). Overall, folds typically verge towards the NE within both the Mearat Sedom Salt Member and Bnot Lot Shales Member, and are consistent with the western (interior) part of the salt wall having moved upwards with a general top-to-the NE sense of shear (Zak and Freund, 1980).

4.2. Minor boudinage within evaporites of the salt wall

Superb examples of minor boudins from within the Mearat Sedom Salt Member are developed along the eastern flank of the Sedom salt wall (Fig. 8a, b). The boudins are composed of marl (e.g. Fig. 8c) and anhydrite (e.g. Fig. 8d, e) layers within the halite, and produce very linear sub-horizontal intersections with bedding (Fig. 8f). This suggests predominantly plane strain conditions with only minor changes in length of the intermediate *Y* axis. The blunt, blocky shape of individual boudins is consistent with a high contrast in mechanical strength between the boudin and halite host (e.g. Ghosh, 1993). Analysis suggests up to 27% vertical extension along individual boudin trains, while Zak and Freund (1980, p. 575) reported a stretching ratio in boudin bearing beds of 1.3–1.6 in a vertical direction. The sense of rotation of individual boudins compared to the orientation of the overall boudin train is clockwise (viewed to the north) (e.g. Fig. 8c, e) and is consistent with the western (interior) part of the salt wall having moved upwards with a general top-to-the NE sense of shear. In addition, some boudins are developed along the eastern margin and south of the central pinched segment of the Sedom salt wall (e.g. Fig. 8g). These boudins also indicate top to the east flow within the salt, but with an additional lateral component consistent with the central part of the salt having flowed south, away from the pinched central segment.

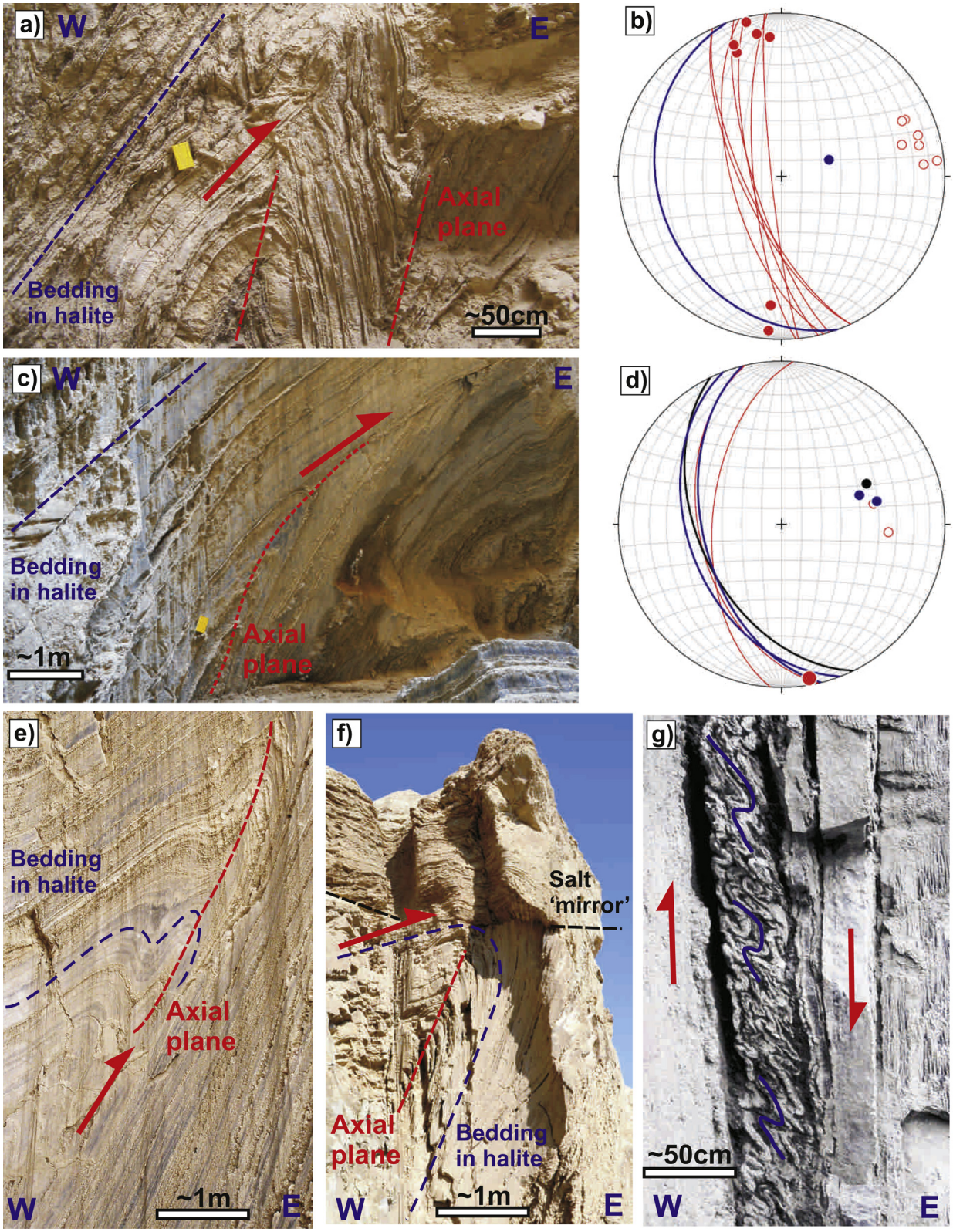

Fig. 6. a) Photographs (a, c) and associated stereonet pairings (b, d) of east-verging folds and thrusts within the Mearat Sedom Salt Member on the NE flank of the Sedom salt wall (N31.101638°; E35.388902°). Photograph a) is a mirrored image. On stereonets, bedding is shown by blue great circles and poles, fold hinges are shown by solid red circles and associated axial planes by red great circles and open circles (poles). In d), the thrust plane is shown by the black great circle and solid black circle (pole). e) East-verging folds and thrust in the Mearat Sedom Salt Member (N31.100593°; E35.389168°), (mirrored image). The position of the salt 'mirror' is marked. f) East-verging folds and thrust in the Mearat Sedom Salt Member (N31.100185°; E35.388722°). g) East-verging folds within thinly bedded Mearat Sedom Salt Member (N31.089147°; E35.393192°) (see Zak and Freund, 1980). The vergence suggests that the interior of the Sedom salt wall has been sheared upwards relative to the margins. Scales is provided by a 20 cm long yellow notebook. (For interpretation of the references to colour in this figure legend, the reader is referred to the web version of this article.)

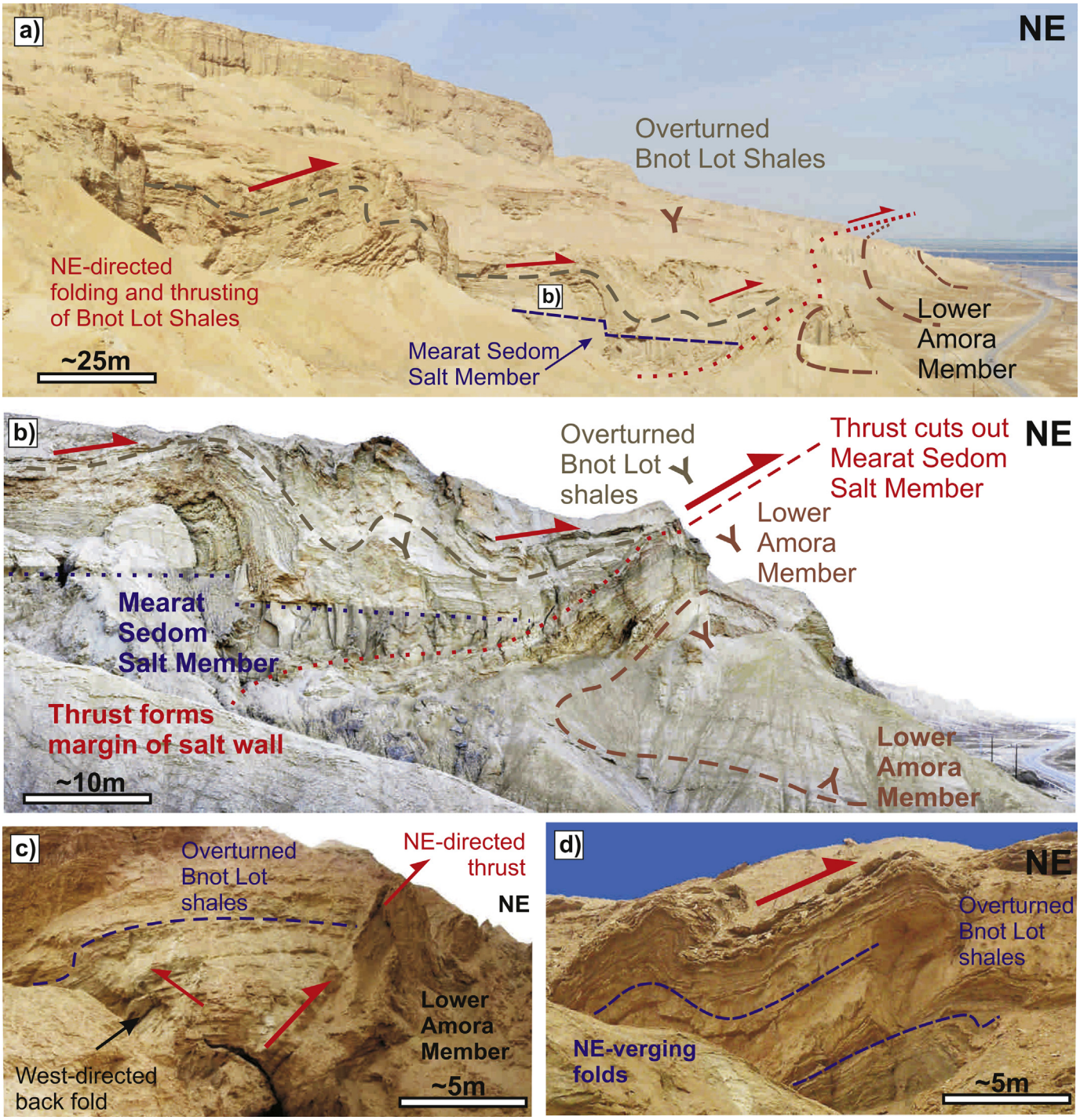

Fig. 7. a) View (looking north) of NE-verging folds and thrusts developed within overturned Bnot Lot shales on the eastern margin of the Sedom salt wall (N31.093458°; E35.390415°). b) Detail showing a NE-directed thrust that cuts out the Mearat Sedom Salt Member and places overturned Bnot Lot shales directly over locally inverted Lower Amora Member shales. Location of photograph b) is shown on a). c) NE-verging thrust carries overturned Bnot Lot shales over the Mearat Sedom Salt Member, resulting in a local west-directed back fold (N31.111681°; E35.390299°). d) NE-verging folds within overturned Bnot Lot shales (N31.098336°; E235.391864°). Photographs c) and d) are mirrored images.

4.3. Minor faults, sediment injections and gypsum veins within the salt wall

The Bnot Lot shales Member is a clastic unit within the salt wall and locally contains minor faults that cut and extend bedding planes (e.g. Fig. 9a–c). Faults typically dip steeply towards the east, and may also define conjugate sets centred about the bedding planes (Fig. 9a, b). Injections of sand have also locally developed in the Bnot Lot shales within the salt wall (Fig. 9d). Injections maintain high angles to bedding and are typically less than 5 cm thick. Extensional fractures associated with injections are also marked by gypsum veining. More extensive systems of gypsum form net vein

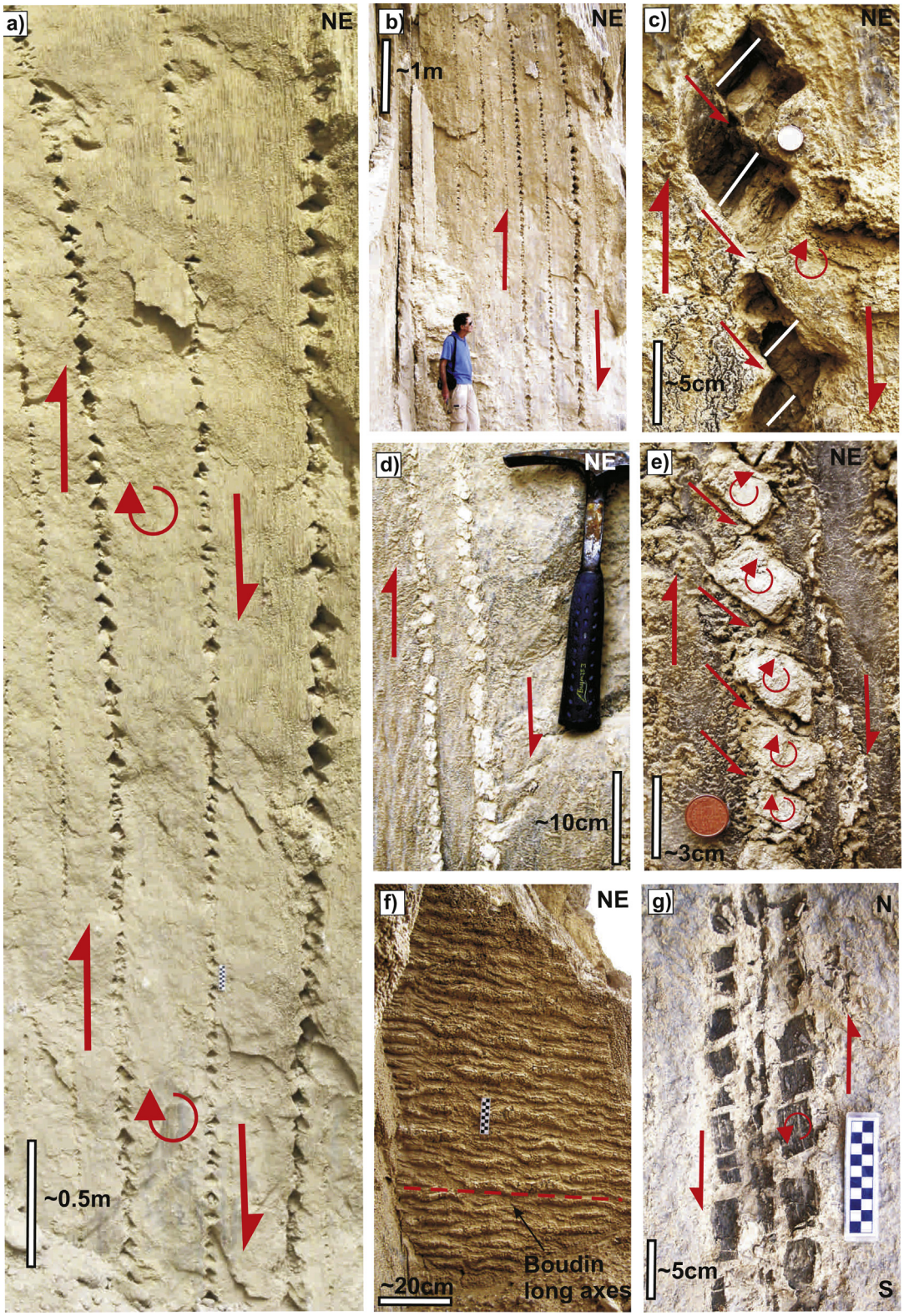

Fig. 8. Photographs of boudins in Mearat Sedom Salt Member (apart from g) from the eastern margin of the Sedom salt wall. All photographs (apart from g) are from the Sedom salt quarry (N31.089147°; E35.393192°), and indicate that the western (interior) part of the salt wall has moved upwards relative to the flanks. The sense of boudin rotation and shear is shown by the red arrows. a, b) Photographs of a vertical boudin-train defined by layers of marl within halite from the Mearat Sedom Salt Member (subsequently destroyed by quarrying). c) Detail of reorientated bedding (highlighted by white lines) within clockwise rotated marl boudins. d, e) Layers of anhydrite within halite of the Mearat Sedom Salt Member. In e) anhydrite boudins display greater clockwise rotation where they become increasingly separated from their neighbours (towards top of photograph). f) View of a foliation plane displaying sub-horizontal intersections of anhydrite boudin necks. g) Plan view of anticlockwise rotated shale boudins in halite from the Hof Shale and Salt Member (N31.08096°; E35.397177°). Sense of rotation suggests salt has flowed towards the south. Scales are provided by a 15 mm diameter coin, a 10 cm long chequered rule and a 30 cm long hammer. (For interpretation of the references to colour in this figure legend, the reader is referred to the web version of this article.)

complexes within the Bnot Lot shales (Fig. 9e). Such complexes are especially well preserved in sandstones and shales immediately above the Mearat Sedom Salt Member. Gypsum veins are up to 75 mm thick, with vertical fibres indicating vertical opening of the fracture/vein system (Fig. 9f). Such veins may interact with one another to form intense systems of 'ladder' fractures over larger (tens of metres) areas of outcrop (e.g. Fig. 9g, h). Thus, sand injections coupled with gypsum net vein complexes indicating vertical 'jacking up' of clastic units collectively suggest that high lithostatic fluid pressures associated with hydraulic fracturing were locally attained within the salt wall (see section 5bii).

4.4. Minor SW verging folds within shales of the salt wall

Minor SW verging folds are locally developed where the Bnot Lot shales Member has more moderate NE-directed dips (mean 145/50NE) in the pinched eastern part of the salt wall (Fig. 10a and b). Hinges of these folds plunge gently to the SE (mean 18/110) and are marked by steep NE-dipping axial planes (mean 133/70NE) (Fig. 10a and b). Larger scale SW-verging folds with moderately NE-dipping axial planes and gently SE-plunging fold hinges locally show evidence of short limbs having faulted and failed during folding (Fig. 10c and d). In addition, mesoscopic folds may detach on underlying surfaces, resulting in SW-verging folds being bound by detachments (Fig. 10e and f). Overall, minor SW verging folds have open angular profiles, are associated with gypsum veining and are marked by brecciation on short limbs, suggesting shales were relatively competent and lithified at the time of this folding.

4.5. Major folding within shales and evaporites of the salt wall

Superb exposure on Mount Sedom reveals that the Bnot Lot shales are folded into a major recumbent fold, here named the Bnot Lot fold. This fold can be traced for 5 km along strike to the north of the 'pinched' central section of the wall, and has an upper limb that can be traced for 500 m across strike towards the east before being obscured by the Dead Sea (Fig. 3 and Fig. 11a, c). Ripple marks (e.g. Fig. 11d), cross laminations (e.g. Fig. 11e), down cutting channels (e.g. Fig. 11f) and graded bedding (e.g. Fig. 11g), developed within shales and sandstones of the Bnot Lot Shale Member enable the way-up of the sequence to be determined. The Bnot Lot shales are clearly shown to young towards the east on the steep limb of the fold, and for the gently westerly dipping limb to be inverted over large areas using a broad range of sedimentary (Zak et al., 1968), geochemical (Zak and Bentor, 1972) and paleomagnetic (Weinberger et al., 1997) criteria. Bedding has been systematically measured around this fold on both the steep right way-up limb (mean 133/77NE) and gentle overturned limb (mean 162/34SW) to define a fold axis that plunges gently towards the NW (15/315) (Fig. 11b). The associated axial plane dips gently towards the north (090/21N) and bisects the acute interlimb angle calculated at ~70° (Fig. 11b). This gently NW-plunging fold may thus be described as a km − scale tight recumbent syncline that faces down towards the NE, with the inverted upper limb of the fold overturning towards the NE. There is a notable lack of minor folds around this large fold displaying systematic vergence towards its hinge. Indeed, folds typically display the opposite sense of vergence to that normally anticipated, with folds on the steep limb verging towards the SW (see Section 4d), whilst those on the gently dipping overturned upper limb verge NE (Section 4a). Differences in outcrop width of the Bnot Lot shales from ~200 m on the steep limb to >400 m on the gentle overturned limb are attributed to variations in gross dip of bedding related to position on the fold, with the true thickness of the shales remaining fairly constant (~200 m) around the closure.

The overturned limb of the fold is unconformably overlain by caprock that mainly comprises anhydrite and gypsum, and is crudely bedded with no evidence of major folding and thrusting (Fig. 12a–c). The observation that caprock is preserved directly on top of clastics of the Bnot Lot Shale Member indicates that salt must at one stage have flowed over the top of the shales prior to dissolution and creation of the caprock (see Section 5a).

The Bnot Lot Shale Member is absent further south (Fig. 3) where it has possibly been cut out by faulting within the salt wall (Zak, 1967), and/or a potential unconformity along the base of the younger Mearat Sedom Salt Member. There is no evidence of a major overturned fold in the salt wall to the south of the central pinched segment. The preservation of pristine sedimentary structures, delicate fish fossils and primary palaeomagnetic vectors demonstrates that despite the tight, recumbent fold geometry, the shales and sandstones show little sign of internal deformation (Weinberger et al., 1997; see discussion section).

4.6. Major extensional faults within shales and evaporites of the salt wall

The margins of the Sedom salt wall are marked by major N–S trending bedding-parallel extensional faults associated with upward movement of the salt, as shown on geological maps (e.g. Fig. 3; Zak, 1967; Zak and Freund, 1980). These faults are outward-dipping away from the salt wall, and are sub-parallel to the steeply dipping salt and overburden along the flanks of the exposed salt wall. However, where the salt is gently dipping towards the west along the eastern flank of the salt wall, then moderately east-dipping faults cut markedly across the bedding, and also transect the overlying caprock (Fig. 3 and Fig. 12d, e). Rotation of bedding in the hangingwall of the fault is consistent with extensional top-to-the east displacement (Fig. 12d, e). These relationships indicate that both bedding-parallel and transecting extensional faults have accommodated upward movement of salt. In addition, the moderately east-dipping extensional fault cuts the overturned limb of the Bnot Lot fold together with the overlying caprock. Hence, it developed after this phase of major folding and dissolution of overlying salt to create the caprock.

4.7. Major variation in thickness of salt members

The Mearat Sedom Salt Member exposed along the eastern flank of the Sedom salt wall displays a pronounced reduction in outcrop width when traced for 200 m along strike, from 380 m in the central pinched region to <20 m on the overturned limb of the Bnot Lot fold (Zak, 1967) (Fig. 3). This variation is all the more remarkable given that the wider outcrop comprises sub-vertical beds, while the narrow outcrop further north dips gently (~20°) towards the west (Fig. 3). Hence, the true variation in thickness is even more extreme and is not a simple artefact of topographic interplay with gently dipping beds.

5. Discussion

5.1. How are large recumbent folds created within a salt wall?

The Bnot Lot shales Member act as a superb marker to define a major tight recumbent fold within the evaporites of the Sedom salt wall. This Bnot Lot fold, which is fully exposed and traceable for 5 km along strike in the northern part of the salt wall, is marked by the NE-directed overturning of the upper fold limb. This results in a completely inverted upper limb that has undergone up to 180° of rotation since deposition, and extends for up to 500 m across strike before being obscured by the Dead Sea (e.g. Fig. 11a). The inverted gently-dipping Bnot Lot shales were locally thrust towards the NE

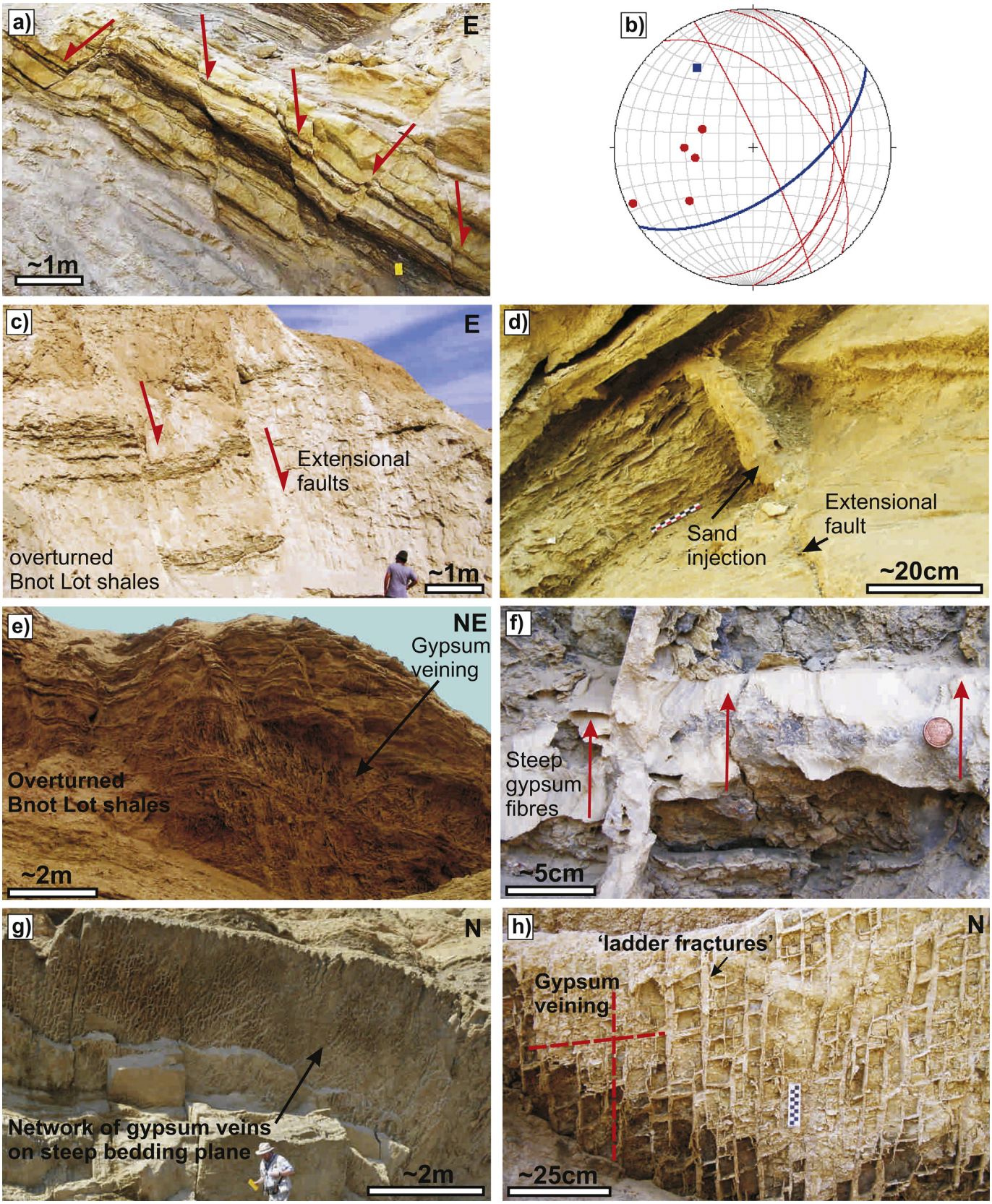

Fig. 9. a) Conjugate extensional faults developed within overturned Bnot Lot shales on the eastern margin of the Sedom salt wall. b) Stereonet of data from a) showing extensional faults ($N = 5$, red great circles and solid red circles representing poles) and bedding (blue great circle and solid blue square representing the pole). c) Extensional faults developed within overturned Bnot Lot shales (N31.090678°; E35.387472°). d) Injection of sand along a normal fault within the overturned Bnot Lot shales (N31.090677°; E35.387178°). e) Intense fracturing with gypsum infill within the Bnot Lot shales close to the underlying Mearat Sedom Salt Member (N31.111681°; E35.390299°). f) Gypsum vein with steep fibres indicating vertical 'jacking up' of overlying sediments, Hof Shale Member (N31.080873°; E35.397298°). g, h) Net vein complex of gypsum veins within the Hof Shale Member (N31.080748°; E35.397472°). Scales are provided by a 15 mm diameter coin, a 10 cm long chequered rule and a 20 cm long yellow notebook. (For interpretation of the references to colour in this figure legend, the reader is referred to the web version of this article.)

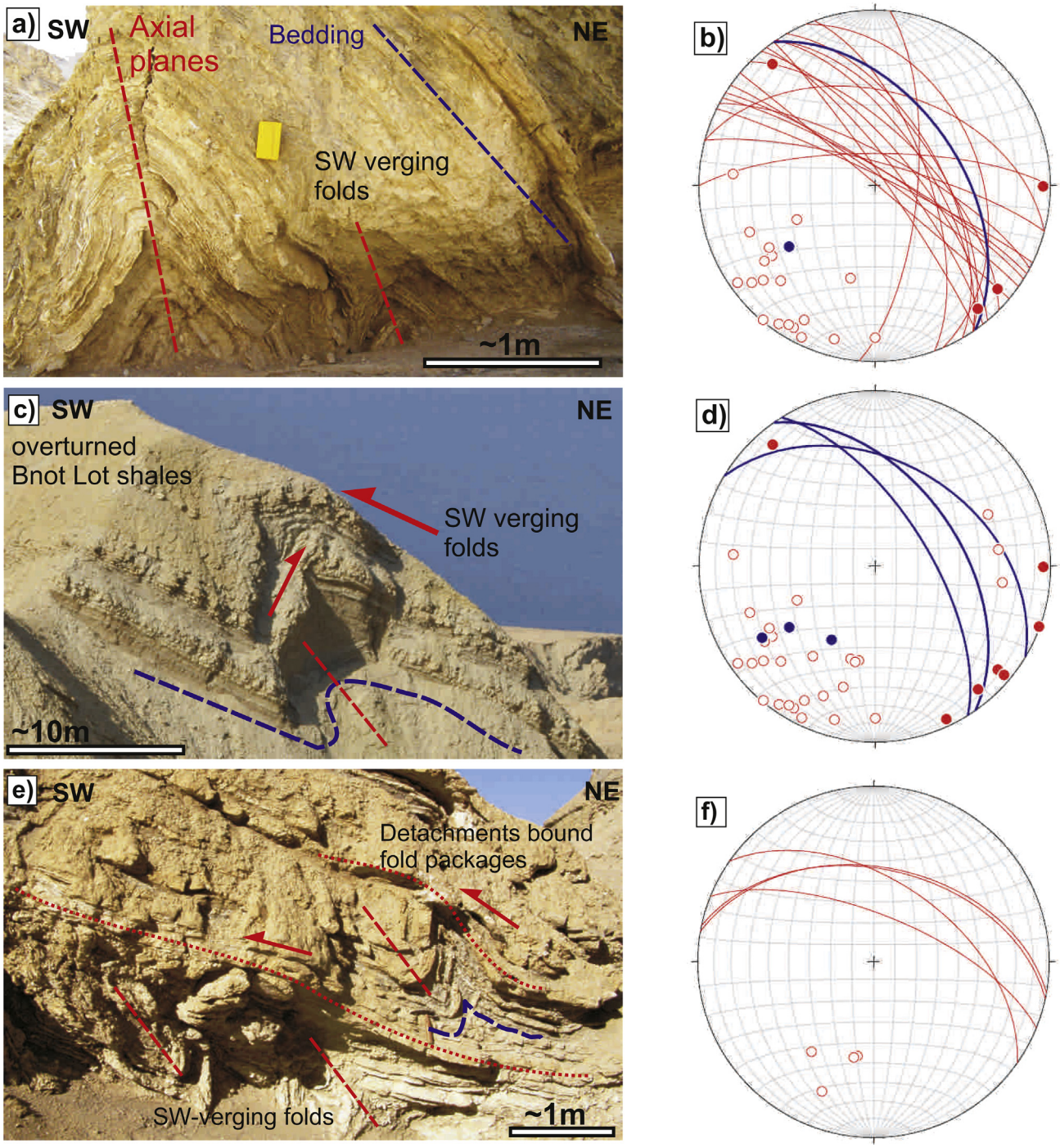

Fig. 10. Photographs and stereonets of SW verging folds formed in the overturned Bnot Lot Shale Member on the eastern part of the Sedom salt wall. a) SW verging folds (N31.087055°; E35.386723°). b) Stereonet of bedding ($N = 2$, blue great circle and blue pole), fold hinges ($N = 4$, red solid circles), axial planes ($N = 19$, red great circles and open red circles representing poles). c) SW-verging folds developed on a 10 m scale (N31.085582°; E35.389345°), (mirrored image). d) Stereonet of bedding ($N = 3$, blue great circles and blue poles), fold hinges ($N = 7$, solid red circles), axial planes ($N = 27$, open red circles). e) Stacked system of SW verging folds detaching on less deformed beds (N31.086402°; E35.388733°). f) Stereonet of fold axial planes shown as red great circles and open red circles (poles). Scales are provided by a 20 cm long yellow notebook and a 30 cm long hammer. (For interpretation of the references to colour in this figure legend, the reader is referred to the web version of this article.)

beyond the margin of the salt wall, to rest directly on top of overturned Amora Formation forming the overburden (e.g. Fig. 7b).

As there is no regional compression along this central part of the Dead Sea Fault system (e.g. Garfunkel, 1981), then folds of this scale and intensity must have been created by processes operating within the salt wall itself. We now discuss three potential mechanisms to generate this fold.

5.1.1. Folding due to flow into the salt wall

Direct examination of mine workings reveals that salt can be intensely folded and deformed as it flows towards, and up the steep neck of the diapir or wall (e.g. Richter-Bernburg, 1980; Talbot and Jackson, 1987; Burliga, 2014). Unless the salt is undergoing internal convection to create a 'mushrooming' effect, this typically results in steeply plunging fold axes, frequently associated with

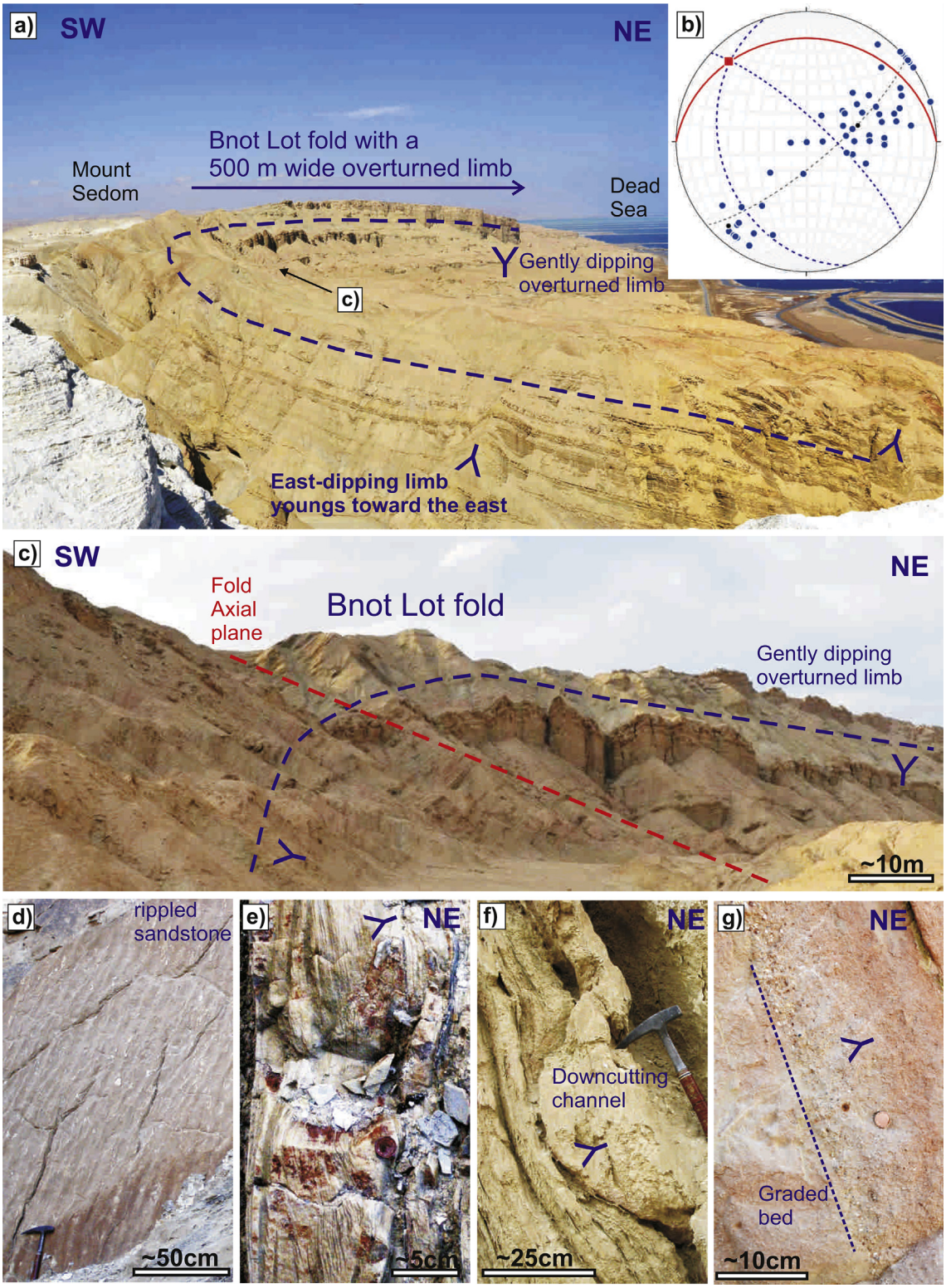

Fig. 11. Photographs from the Bnot Lot Shale Member within the Sedom salt wall. a) Bnot Lot fold with a 500 m wide inverted upper limb (as shown by the "Y" younging symbols). b) Stereonet of poles to bedding ($N = 60$, solid blue circles) measured around the Bnot Lot fold, together with mean fold limbs (dashed blue great circles), calculated profile plane (black dashed line), calculated fold hinge (red square at 15/315)) and axial plane (solid red line at $090/21^{N}$). c) Hinge area of the Bnot Lot fold, with bedding passing from steep to gently-dipping and overturned around the fold hinge. Location of photograph shown on a) (N31.088998°; E35.387772°). d) View onto the top of a bedding surface displaying ripple marks and younging to the east (N31.086917°; E35.389908°). e) Cross laminations indicating younging to the east (N31.086348°; E35.392520°). f) Channel cutting down into underlying shales indicating younging to the east (N31.086425°; E35.391427°). g) Graded bedding within coarse sandstones indicating younging to the east (N31.086438°; E35.391433°). Scales are provided by a 30 cm long hammer and a 15 mm diameter coin. (For interpretation of the references to colour in this figure legend, the reader is referred to the web version of this article.)

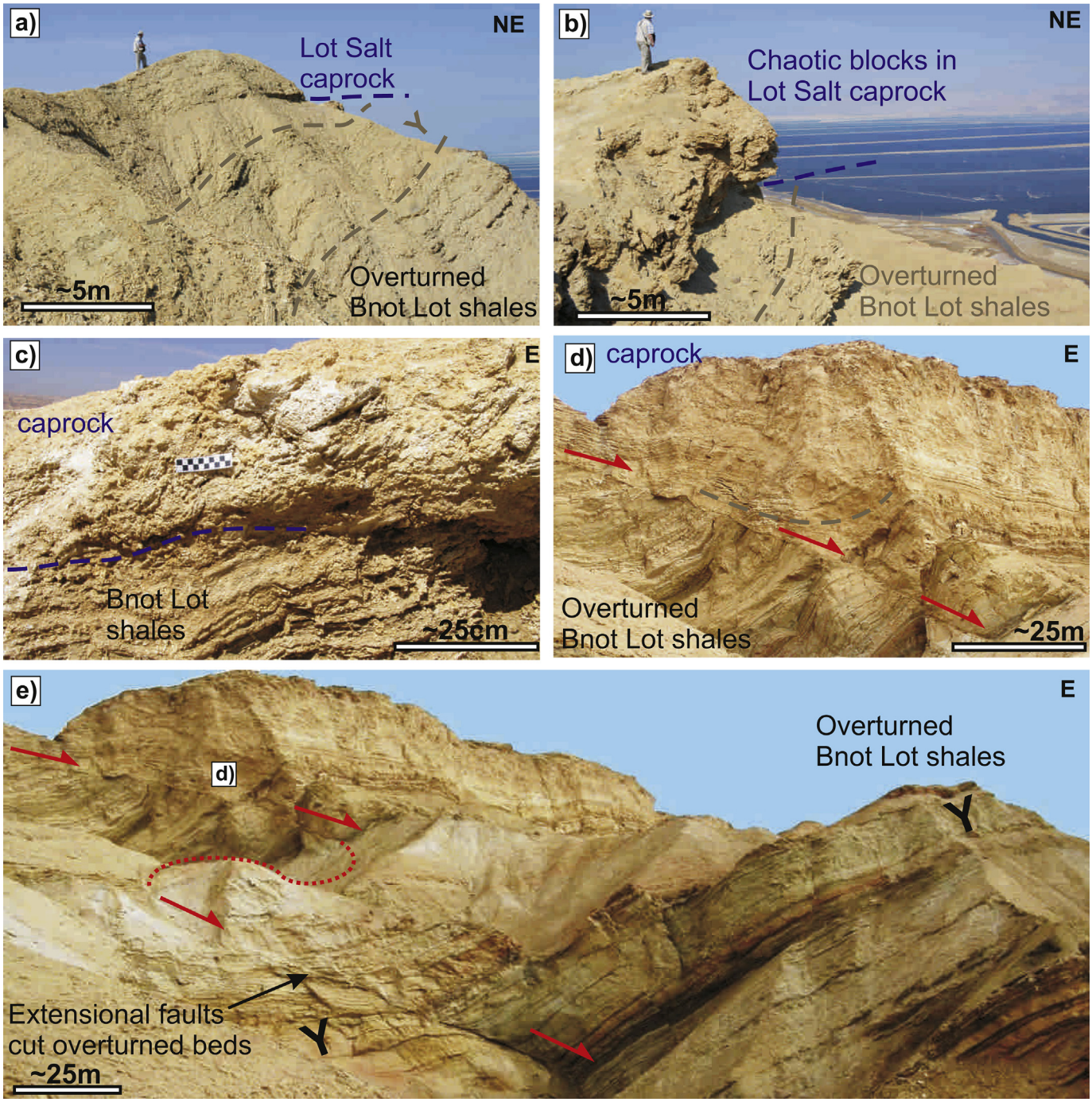

Fig. 12. Photographs of moderately-dipping overturned beds within the Bnot Lot shales that are overlain by caprock derived from Lot Salt member (a) (N31.090147°; E35.385572°), that displays chaotic blocks (b) (N31.092168; E35.385357°), and a sharp lower contact (c) (N31.092067°; E35.385355°). d, e) Large extensional fault cutting caprock and moderately west-dipping (overturned) Bnot Lot shales on the eastern margin of the Sedom salt wall (mirrored images) (N31.091238°; E35.387475°). Beds in the hanging wall of the fault have rotated towards the fault plane, confirming extensional top-to-the east displacement. Location of photograph d) is shown in e). Scale in c) is provided by the 10 cm long chequered rule.

constrictional deformation (e.g. Jackson and Talbot, 1989). In addition, Jackson et al. (2014) suggest that some folding imaged within salt walls may be driven by Raleigh–Taylor instabilities, where anhydrite-rich horizons overlie less dense halite-dominated units. There is however no evidence within the Sedom salt wall for such, thick anhydrite-rich horizons to create instability. In summary, the recumbent and gently plunging nature of the major Bnot Lot fold within the Sedom salt wall, the single sense of overturning towards the NE, and the impure nature of the evaporite sequence effectively precludes the internal salt flow and convecting mushroom model.

5.1.2. *Folding due to salt dissolution and collapse*

The Bnot Lot shales form a major clastic unit bounded on the W and E sides by evaporites of the Lot Salt Member and Mearat Sedom Salt Member, respectively (Fig. 3). While these moderately-dipping

halite-rich members may undergo dissolution resulting in a lowering of the surface level, the intervening clastics are non-soluble and would therefore start to form an upstanding linear ridge. With continued dissolution of surrounding salt, the ridge formed of Bnot Lot shales may eventually start to undergo gravity-driven collapse back downslope towards the NE. This could result in complete overturning of the upper fold limb as the fold tightens. Although the inverted limb is exposed for 500 m across strike, the dissolution and collapse would have been a gradual progressive process, and there is no necessity in the model for the clastic ridge to have been this height at any time. Thus, the limb would be incrementally inverted as surrounding salt was progressively dissolved, with the width of the inverted limb (500 m) thereby providing an overall estimate of the vertical thickness of salt dissolved.

However, the Bnot Lot shales form a pristine sedimentary sequence with very little internal fracturing. The overturned limb would be especially disrupted if it had undergone collapse as envisaged in the model. The steep limb and overturned limb display the same limited amount of deformation, and there is no evidence of enhanced fracturing related to collapse. In summary, although the Bnot Lot shales may very locally have undergone a small component of collapse to rest directly on top of the structurally underlying Mearat Sedom Salt Member and its caprock (e.g. Zak, 1967), this process cannot adequately explain the overall km-scale folding observed within the salt wall.

5.1.3. Folding due to salt sheet emplacement

The Bnot Lot fold exposed at the surface is a tight recumbent syncline with a calculated interlimb angle of ~70° as measured between the steep dips of the salt wall and overturned limb (Fig. 11b). However, the true amount of overturning is much greater, with inverted horizontal beds of the upper limb indicating a 180° overturn from original depositional orientations, as first recognised by Zak et al. (1968). Such extreme folding has been imaged on seismics, both in the overburden (e.g. Hudec and Jackson, 2006) and directly within evaporitic salt walls themselves (e.g. Jackson et al., 2014). In these cases, salt is inferred to have formed a sub-horizontal sheet that flowed laterally, thereby causing overturn of the underlying layers to create recumbent fold limbs described as 'flaps' by Graham et al. (2012) and Jackson et al. (2014). The scale of inverted limbs may extend to several km (e.g. Graham et al., 2012), although outcrop examples are currently restricted to about 500 m (e.g. Davison et al., 1996).

Within the Sedom salt wall, complete overturning of the Bnot Lot shales to define the inverted upper limb could be generated by the more mobile Lot Salt Member (exposed to the west) having partly extruding to the NE over the top of the shales. Folding of the shales is generated by shear traction as salt flowed over the top, together with a component of gravity as both salt and shales moved downslope towards the NE. In this respect, it is important to note that the 315° orientation of the Bnot Lot fold hinge (Fig. 11b), is oblique to the N–S trend of the salt wall, but is broadly parallel to the calculated 310° strike of the regional palaeoslope inferred from slump folding in the younger Lisan Formation (Alsop and Marco, 2012). The NE-directed sense of overturning is thus entirely consistent with downslope movement of an overlying salt sheet towards the depocentre of the basin. The minimum 500 m width of the overturned limb is also consistent with the scale of overturned limbs from existing seismic and outcrop studies. The source of the outflowing salt to the west of the Bnot Lot shales is in accord with the studies of Weinberger et al. (2006a) who suggested that the Sedom salt wall was sourced primarily by salt flowing from the east, with only a minor component being derived from the west. The convergence of flow from these two evaporite sources results in a 'suture' down the spine of the Sedom salt wall and to the west of the Bnot Lot shales (Frumkin, 1996c; Weinberger et al., 1997). In general, although salt may be subsequently dissolved to leave little record of such recumbent fold limbs in older settings, clastic units are insoluble and may therefore retain a more complete structural history of adjacent salt kinematics and flow.

5.2. What are the kinematics and mechanics of recumbent folds within a salt wall?

In terms of general kinematics, folds are widely interpreted as having either, a) a hinge that remains fixed with respect to its position on fold limbs; or, b) a hinge that is able to migrate along the folded layer. Although these respective 'fixed hinge' and 'rolling hinge' fold models have been previously developed to explain large-scale recumbent folds within orogenic belts (e.g. Platt, 1982; Butler, 1992), they have more recently been applied to salt sheets (e.g. Graham et al., 2012).

5.2.1. Fixed hinge fold model

If we apply the fixed hinge model to the Bnot Lot fold that contains a >500 m wide overturned limb, then this would necessitate this limb to have originally extended for 500 m vertically, before rotating around the fixed hinge to create the overturned sequence observed today. If the overturned limb was created deeper within the salt wall and subsequently carried toward the surface, then the issue becomes one of how it was locally able to thrust through the flank of the salt wall and directly into the overburden (Fig. 7a, b). The overturned limb would then have to maintain, pristine high-angle thrust cut-off relationships with the overburden, despite being carried to the surface in the high-strain sheared margin of the salt wall (Zak and Freund, 1980). In addition, the correspondence of the Bnot Lot hinge trend with the strike of palaeoslope would be entirely fortuitous. Conversely, if the fold limb was created at or near the surface, then studies have shown that without significant regional contraction, salt is unable to support surficial relief of more than 300 m (e.g. Davison et al., 1996), and certainly not the 500 m that would be required to create the observed width of the inverted limb in a fixed hinge model. Thus, a 'fixed hinge' model seems unlikely and we therefore now consider a 'rolling hinge' model.

5.2.2. Rolling hinge fold model

Rolling hinges, which have been likened to beds of rock passing around the hinge as if forming part of a 'tank track' have been suggested to create inverted limbs within salt flows (e.g. Talbot, 1979, 1998) and overturned sequences within overburden to salt by Graham et al. (2012). The ability of the hinge to migrate relative to the limbs removes the necessity for the inverted limb to have formed with a width of 500 m. Thus, the salt wall need never have attained a surface relief of 500 m. Indeed Graham et al. (2012) suggest that salt need not be uplifted much above regional in such a model. Thus, the width of the overturned limb simply reflects the minimum amount of salt that has flowed around the hinge and into the inverted limb (downslope towards the NE). This may explain the lack of systematic minor fold vergence towards the hinge, with individual minor folds passing around the hinge from the steep limb to the overturned limb. It is noteworthy that a similar lack of consistent minor fold vergence has also been recorded from adjacent to other extrusive salt sheets (e.g. Davison et al., 1996).

As the Sedom salt wall has been asymmetrically sourced, with salt flow predominantly from the basin to the east, there is no correlation of Sedom Formation stratigraphy across the salt wall. The consequence of this is that the salt never defined a simple

anticlinal shape, as would be associated with the leading edge of a rolling tank track (e.g. Graham et al., 2012) (Fig. 13a). Rather, the asymmetric sourcing from the basin resulted in the Bnot Lot fold being overrun by the salt sheet. This led to the upper overturned limb rolling forwards towards the east to create a tight synclinal hinge, as if at the rear of a rolling tank track (e.g. Graham et al., 2012) (Fig. 13b). The implication of this 'rear tank track model' is that the Lot and Mearat Sedom salts broke out relatively early (because of asymmetric sourcing) and occurred towards the crest of the salt wall, rather than along the hinge of an attenuated anticline somewhere to the east (Fig. 13b).

Existing studies of sediments forming overturned folds adjacent to proposed salt sheets (e.g. Richter-Bernburg, 1980), characteristically describe pristine logged relationships (e.g. Davison et al., 1996, p. 35) and note that they are "not internally deformed" (e.g. Graham et al., 2012, p. 599). This characteristic lack of internal strain, despite overturning associated with tight to isoclinal folding, is also present in the Bnot Lot shales, where sedimentary structures indicating inversion have long been recognised (e.g. Zak et al., 1968). The lack of pronounced fracturing and faulting in the Bnot Lot shales around the hinge and overturned limb of the fold suggests that the shales were mechanically weak, especially considering the rates at which the salt may have flowed to create the fold. The observation of sedimentary injections and gypsum veining within the Bnot Lot shales (e.g. Fig. 9), indicates that significant overpressuring may have existed that would inherently weaken the shales and facilitate folding. Injection of sands requires a sustained pressure difference between the source layer and the propagating fracture, which leads to dilation of the fracture thereby enabling the sand-water mixture to flow through the fracture (Levi et al., 2008). Price and Cosgrove (1990, p. 369) note that folding occurs at strain rates many times greater than would allow time for the release of fluids, thereby leading to fluid overpressuring. They summarise their findings by noting that "it is to be expected that high fluid pressures will obtain during folding". We therefore suggest that the Bnot Lot shales were mechanically weak during recumbent folding due to overpressuring enhanced by the seal created by the surrounding impermeable evaporites. The folding of the Bnot lot shales is thus considered to be in direct response to flow and gravity-driven lateral extrusion of salt towards the NE within overlying evaporites.

5.3. *Why are outward-verging folds created on the flank of a salt wall?*

NE-verging folds and thrusts are observed along the eastern margin of the Sedom salt wall, particularly to the north of the central pinched segment, but are absent from the western flank. They are especially well developed in the Mearat Sedom Salt Member, as well as in the overlying Bnot Lot shales (Fig. 7). In some instances thrusts have cut through the Mearat Sedom salt and caprock and have carried the Bnot Lot shales directly onto the overturned Amora Formation (e.g. Fig. 7a, b). There are three general processes which could create these NE-verging folds and thrusts.

5.3.1. *Slump fold model*

NE-verging slump folds are observed along the western side of the Dead Sea Basin, where sediments have slumped downslope towards the depocentre of the basin (Alsop and Marco, 2011, 2012, 2013, 2014). However, on the eastern margin of the Sedom salt wall, the caprock and overlying Bnot Lot shales locally dip gently to the west (e.g. Fig. 7d), rather than to the east as would be required to generate NE-verging slump folds and thrusts. Subsequent uplift of the Sedom salt wall can only have reduced these westerly dips rather than exaggerating them. In addition, the presence of gypsum and anhydrite in caprock would have encouraged early cementation and lithification that would limit the opportunity for soft-sediment folding related to slumping. The observation that NE-verging folds and top-to-the NE thrusts are also developed in the underlying Mearat Sedom Salt Member (e.g. Fig. 6), where they could not be created by slumping, forces us to consider a second mechanism.

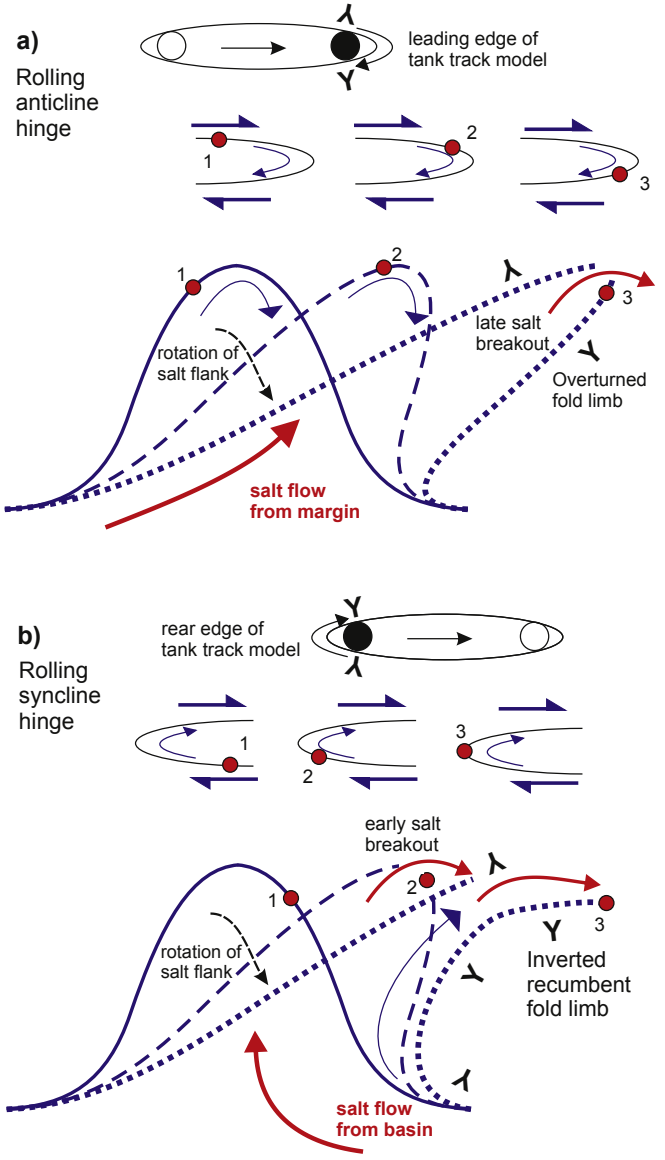

Fig. 13. Schematic cartoons (modified from Graham et al., 2012) showing alternative recumbent fold models involving a) a rolling anticline hinge developed at the leading edge of a hypothetical 'tank track' and resulting in relatively late salt breakout, and b) a rolling syncline hinge developed at the rear edge of a 'tank track' and resulting in early salt breakout. Progressive stages in the evolution of the top salt surface are shown by solid, dashed and dotted blue lines respectively. The migration of a point on fold limbs is shown by a red circle, direction of younging by the 'Y' symbol, and overall salt flow by red arrows. Both models result in a downslope component to salt flank rotation. (For interpretation of the references to colour in this figure legend, the reader is referred to the web version of this article.)

5.3.2. *Ghost fold model*

Folds preserved within the caprock could have originated as NE-verging folds within the underlying Mearat Sedom Salt Member

(Zak, 1967). There is some evidence that impure layers within the salt are preserved when the surrounding halite-rich salt is dissolved (e.g. Zak, 1967). However large folds in salt are unlikely to be preserved in the caprock as steep and gentle fold limbs would vertically collapse at different rates leading to a more chaotic structure. In addition, given that a relatively thin caprock requires a large initial thickness of salt to be dissolved, then folds in salt would originally require very large amplitudes (10's of metres) to survive. The observation that folds in the caprock contain detailed relationships such as an axial-planar foliation together with parasitic fold hinges effectively precludes the 'ghost fold' mechanism as a major factor, although it could have generated small isoclinal folds.

5.3.3. Tectonic fold model

Having effectively eliminated the slump fold and ghost fold models as major mechanisms, we now consider a more general tectonic model driven by the Sedom salt wall itself. The broad observation that NE-verging folding and thrusting affected all units including salt, caprock, overlying Bnot Lot shales and Amora Formation, but was restricted to the basinward (eastern) flank of the salt wall, leads us to now evaluate the role of salt extrusion in forming these structures.

A salt sheet sourced from the Lot Salt Member forming the crest of the salt wall is considered to have been extruded towards the NE, and flowed downslope towards the depocentre of the basin (Fig. 13b and Fig. 14, see previous section). This created the large scale recumbent fold and inversion of the underlying Bnot Lot shales. The NE-verging folds and thrusts recognised in the Bnot Lot shales along the eastern flank of the salt wall are interpreted to have been superimposed on the already inverted limb of the major fold, as; a) they also fold the directly underlying caprock, and; b) NE-verging thrusts have locally cut the Mearat Sedom Salt Member and its caprock, and have emplaced overturned Bnot Lot shales directly onto Lower Amora Member forming the overburden to the salt wall. The superimposition of folds and thrusts verging away from the salt body on an already entirely inverted sequence is also interpreted from outcrop studies below other salt sheets (e.g. Davison et al., 1996). In addition, thrusts and shears directed away from the salt wall and extending into the adjacent overburden are also imaged on seismic sections of salt walls (e.g. Jackson et al., 2014). These shear zones typically develop slightly below the crest of the wall (Jackson et al., 2014), and are therefore in a similar position to those observed in the present study that are ~200 m below the crest of the Sedom salt wall. Although Jackson et al. (2014) attribute such thrusts and shears to a regional contractional overprint, there is no evidence in the present study for such an event. We therefore suggest that outward-directed folds and thrusts in the Sedom salt wall were created by gravity-driven lateral flow of salt.

5.4. How is overturned salt dramatically thinned on the flank of a salt wall?

The Mearat Sedom Salt Member, forming the eastern flank of the Sedom salt wall, displays a ×20 reduction in thickness from 380 m on the steep limb of the Bnot Lot fold to just <20 m where it is exposed on the overturned limb of this fold (Fig. 3). This is all the more remarkable considering that this reduction occurs over a strike length of just 200 m. We discuss a number of potential mechanisms that may account for this extreme geometry.

5.4.1. Salt dissolution

It could be argued that the pronounced reduction in thickness of the Mearat Sedom Salt Member was created via dissolution and removal of salt in solution. However, we do not consider this to be the major process as a) the caprock overlying the thin, overturned salt is no thicker than that covering the much thicker (>1000 m) salt sequence further south (Fig. 3; Zak, 1967), b) it is unclear as to why overturned salt would have undergone significantly more dissolution.

5.4.2. Tectonic excision via normal faulting

Although steep normal faults are locally present along the eastern side of the Mearat Sedom Salt Member (Zak, 1967) and may cut out some of the salt thickness, they fail to produce significant brecciation or fracturing and do not appear large enough to have removed 100's of metres of sequence in such a short distance. Furthermore, with such a mechanism it is difficult to envisage a) the coincidence of thinning of the Mearat Sedom Salt Member with position on the overturned limb of the Bnot Lot fold; b) why steep normal faults which cross cut and transect 100's m of stratigraphy would fortuitously leave a continuous thin (~20 m) sliver of Mearat Sedom salt exposed for more than 4 km along strike to the north.

5.4.3. Tectonic excision via thrust faulting

The base of the overturned Mearat Sedom Salt Member is in places marked by an NE-directed thrust that has carried the inverted Lot Salt and Bnot Lot Shales sequence directly over Amora Formation. This has produced distinct stratigraphic cut-offs in the footwall to the thrust, and if the thrust were to have ramped through the salt in the direction of thrust transport towards the NE, then it could have significantly reduced the thickness of the Mearat Sedom Salt Member. Although this mechanism is possible, it should be noted that; a) when thrust faults enter salt horizons, they typically display very long flat segments rather than ramps (e.g. Butler et al., 1987), b) the excision of >350 m of salt over a horizontal distance of just 200 m makes this thrust ramp model highly unlikely.

5.4.4. Tectonic extrusion (via loading)

The NE-verging folds and thrusts in the Mearat Sedom Salt Member suggest that it could have been partly attenuated and 'squeezed out' during overall NE-directed shearing. Indeed, the 20 m thick outcrop of the Mearat Sedom Salt is typically marked by a pronounced NE-closing recumbent antiform (Fig. 6e, f). The coincidence of rapid thinning of the salt with the hinge and overturned limb of the Bnot Lot fold suggests that the salt may have been extruded due to the increased overburden created by the fold itself. Attenuation and evacuation of the Mearat Sedom Salt Member from the hinge and overturned limb of the Bnot Lot Fold would have allowed the fold to progressively tighten and rotate while remaining relatively low strain. Thus, the inverted limb of the fold was sheared over towards the NE by the overlying Lot Salt Member, while the underlying Mearat Sedom salt was attenuated and extruded to create NE-verging folds and thrusts. In such a scenario, it is interesting to note that in subsurface settings, the ~20 m of overturned Mearat Sedom salt forming the base of the lateral extrusion would be difficult to image given the resolution of most seismic sections. Major recumbent folds that face towards the margins of the salt wall have however been recently identified on seismic sections by Jackson et al. (2014), who note that the base of the allochthonous salt sheet is "discordant with underlying but younger evaporites" that are recumbently folded. Thus, the development of the overturned recumbent fold limb in a strike distance of <200 m is in general accord with existing seismic analysis.

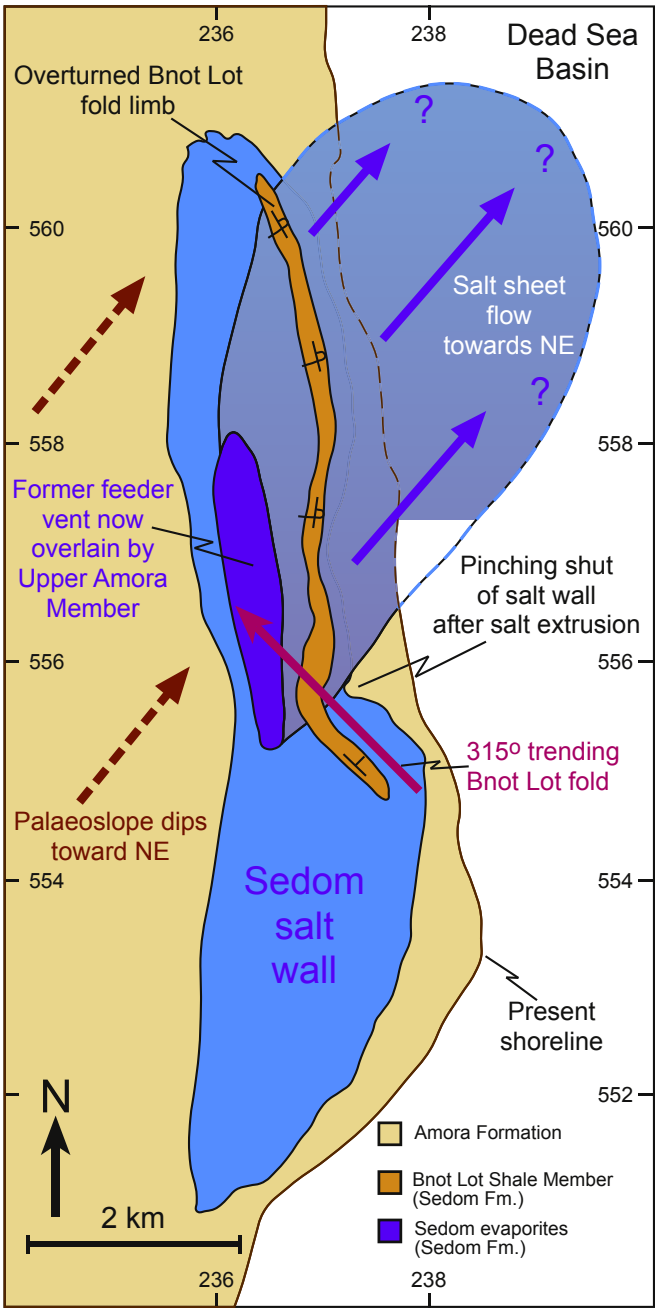

Fig. 14. Schematic map illustrating the position and extent of the former salt sheet flowing from the Sedom salt wall at ~420 ka. This salt sheet is interpreted to have flowed down the palaeoslope towards the NE and the depocentre of the basin. It resulted in the creation of the recumbent 315° trending Bnot Lot fold marked by an overturned upper limb. The vent subsequently pinched closed and was covered by the Upper Amora Member. See text for further discussion.

5.5. What creates the pinched 'hour-glass' shape of a salt wall

The 'hour-glass' shape of salt walls, where the lateral terminations are wider than the central segment (e.g. Rowan and Vendeville, 2006) have been previously termed a 'Q-tip' shape by Rowan et al. (2012). These authors describe an extreme situation where the central portion of the salt wall has entirely closed, to create a vertical salt weld. They attribute this to superimposed regional contraction with the thickest part of the original salt wall suffering the greatest amount of squeezing thereby resulting in it being pinched shut. The 10 km long Sedom salt wall also displays a characteristic hour-glass pattern in map view, with a narrow 2 km long central section being just ~40% of the width of the northern and southern segments (Fig. 3). However, the lack of regional contraction in the central part of the strike-slip dominated Dead Sea Fault system means that this contractional model is not considered suitable for the Sedom salt wall.

In order to consider alternative models, it is useful to note that the central 'pinched' area of the Sedom salt wall is just 800 m wide at the surface and coincides with:

a) *A reduction in dip of the NE-dipping Bnot Lot shales coupled with SW verging folds*. The Bnot Lot shales in the eastern part of the pinched segment display a progressive reduction in dips over ~500 m from subvertical attitudes to moderate dips (~50°) towards the NE. This reduction in the angle of dip coincides with the development of SW verging folds in the Bnot Lot shales that are considered to have formed relatively late as they have angular (almost chevron-like) profiles with breccia developed along associated fault planes. These folds are restricted to the pinched region where the beds dip moderately NE.

b) *A zone of overturning within the salt wall marked by the Bnot lot shales*. The overturned limb of the previously described Bnot Lot fold also developed in the central pinched area and extends northwards for 5 km. This fold is a major structure within the salt wall and the notable coincidence of the recumbent fold and pinched area suggests that these two features may be mutually related.

c) *A 40° anticlockwise rotation of palaeomagnetic overprints within the eastern part of the Sedom salt wall*. Based on palaeomagnetic overprints, Weinberger et al. (1997) suggested a relatively late stage 40° anticlockwise rotation of the Sedom salt wall in the pinched region. This late stage rotation occurs after the beds had already been tilted into steeply-dipping attitudes within the salt wall. It is notable that this rotation is observed on the eastern side, but not the western side of the Sedom salt wall. Although Weinberger et al. (1997) invoked 'external' forces linked to the Dead Sea Fault system to produce such a rotation, this is difficult to reconcile with the observation that only the eastern part of Sedom salt wall was affected and the western flank does not display such a rotation.

d) *A rotation in the strike of Lower Amora Member beds flanking the eastern margin of the salt wall*. The strike of bedding within the Lower Amora Member that flanks the eastern margin of the salt wall displays an anticlockwise rotation from typical N–S trends to more E–W orientations in the pinched area (Fig. 3). As the Lower Amora Member forms part of the overburden, then it is clear that the pinching process affected the salt wall and overburden alike, and took place after deposition of the Lower Amora Member.

e) *The greatest preservation of Amora Formation resting directly on top of the salt wall*. The greatest preservation of Upper Amora Member sandstones and shales deposited directly on top of the Sedom salt wall occurs in the central pinched area of the salt wall (Fig. 3). There is effectively no Amora Formation preserved above the southern segment of the salt wall, while the northern section is also typically devoid of overlying Amora Formation (Fig. 3). The Upper Amora Member is therefore largely restricted to overlying the central ~3 km of the salt wall (Fig. 3 between Grid northings 555 and 558) where pinching and narrowing of the wall has occurred.

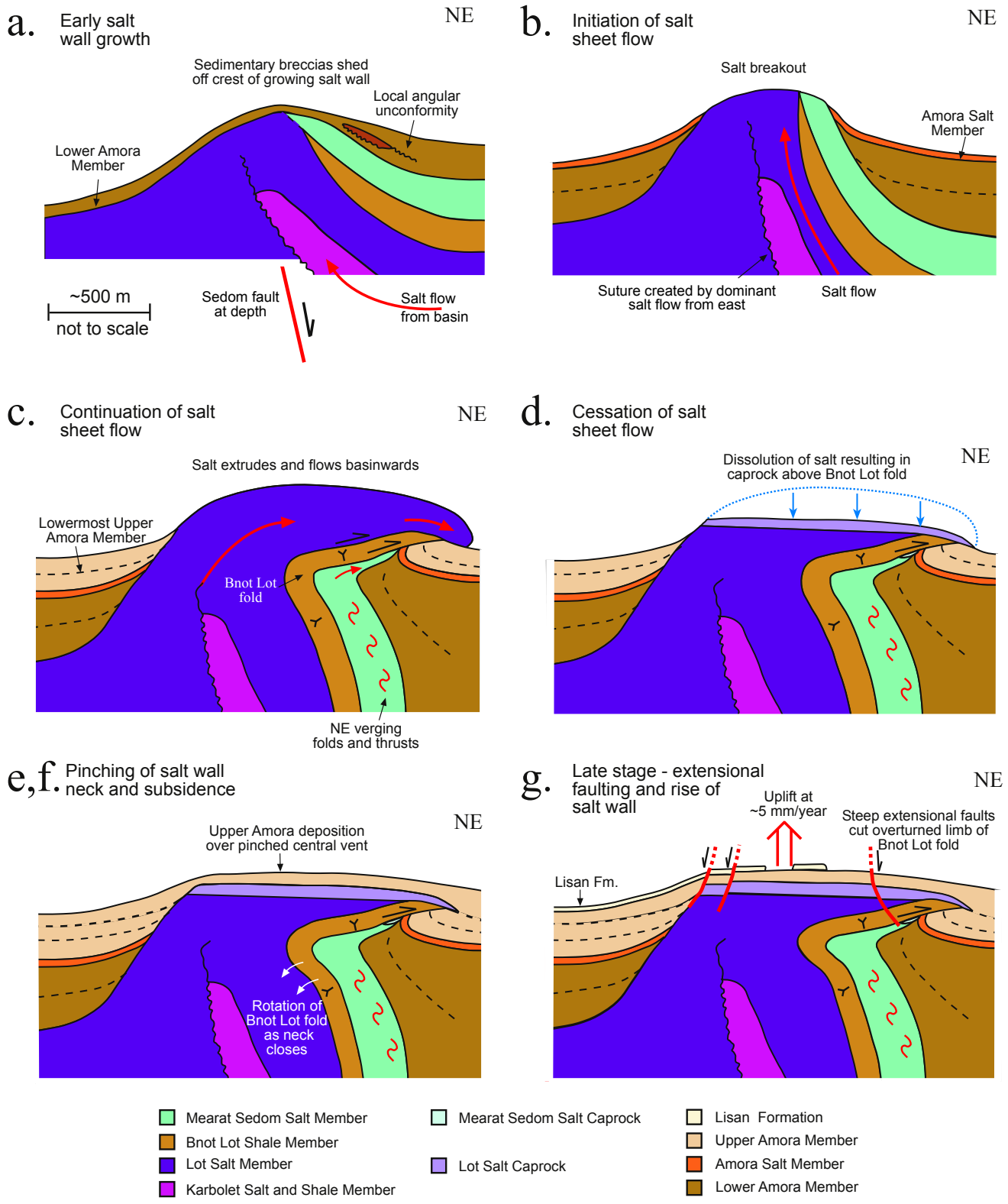

Fig. 15. Schematic cartoons illustrating the evolution of the central and northern portion of Sedom salt wall and associated salt sheet. NE–SW trending sections are not to scale and are drawn through the central part of the salt wall. a) Early salt wall growth marked by salt flow from the east, leading to local unconformities and shedding of Lower Amora sediments off the rising salt crest. b) Initiation of salt sheet flow at ~420 ka, with significant development of salt wall relief ultimately leading to salt 'breakout' above the crest of the central salt wall. c) Continuation of salt sheet flow resulting in the generation of the recumbent Bnot Lot fold as salt extrudes towards the NE and the depocentre of the basin. d) Cessation of salt sheet flow marked by dissolution of the overflowing Lot Salt Member and creation of caprock above the Bnot Lot fold. e, f) Pinching of the central salt wall as the supply of salt reduces, resulting in rotation towards the SW of the Bnot lot fold. This was followed by continued subsidence above the central area of the salt wall, leading to deposition of Upper Amora Member directly above the former salt neck. g) Late-stage extensional faults cut both margins of the salt wall, as well as caprock and the Upper Amora Member as salt continues to rise.

We now attempt to link these observations in to a general model relating to the evolution of the Sedom salt wall, and in particular the central pinched section of this structure. As the Bnot Lot shales are overturned in the central segment, we propose that this area may have been the source of the Lot salt sheet that flowed towards the NE over the top of the shales (Fig. 14, see previous section 5c). However, following the outflow of salt, we envisage that the central section of the salt wall was closed back in on itself due to the removal of salt from the former vent via extrusion and/or dissolution. The moderate NE dips, late SW verging folds, and bulk 40° anticlockwise rotation shown by palaeomagnetics would support this closure. The fact that the Amora Salt Member, together with part of the immediately overlying Upper Amora Member strikes NW–SE within the overburden on the eastern margin of Sedom suggests that any collapse and pinching process (associated with rotation) continued for some time after their deposition. The collapse and "fall" of central Sedom resulted in subsidence, leading to the thickest sequence of the Upper Amora Member being deposited and preserved directly on top of this region of the Sedom salt wall.

Recent analysis of seismic sections led Jackson et al. (2014) to suggest that evacuation of salt into allochthonous sheets resulted in 'foundering' of the original anticline forming the salt wall. In the Sedom salt wall, we propose that there is evidence not only for a salt sheet, but also the potential pinching and closing of the source of the salt sheet after its outflow, leading to subsidence. This would have to occur before deposition of the Upper Amora Member that unconformably rests directly on top of the caprock of the Sedom salt wall.

6. Model of salt wall evolution

We now outline an evolutionary model for the development of the Sedom salt wall with some general time constraints provided by stratigraphic relationships and associated isotopic dates.

6.1. Stage 1 – early salt wall growth (Fig. 15a)

The Sedom Formation comprises a series of Late Miocene-Pliocene evaporites named the Karbolet Salt and Shale Member, Lot Salt Member and Mearat Sedom Salt Member (Table 1). While the N–S trending Sedom salt wall appears to be controlled by the underlying Sedom Fault of similar trend (Figs. 1b and 2), the exact age of initiation salt wall growth remains poorly constrained. It appears to have influenced deposition of the overlying Pleistocene clastics forming the Amora Formation (Weinberger et al., 2006a). These Pleistocene deposits are much thicker towards the east, suggesting that most of the salt that fed into the growing Sedom salt wall was sourced from the east and the centre of the basin (Figs. 2 and 15a). Proximal sedimentary breccia layers observed within the Lower Amora Member (Fig. 5a–c), are interpreted to have been shed off the eastern flank of the growing salt wall, suggesting that it had bathymetric expression during deposition of this member at around 740 ± 66 ka (U series ages from Torfstein et al., 2009). Dissolution of salt to create caprock may thus have commenced during deposition of the Lower Amora Member. The siting and initiation of Sedom salt wall is interpreted to have been controlled by the Sedom Fault, with subsequent development via passive diapirism in the Pleistocene (Fig. 15a).

6.2. Stage 2 – initiation of salt sheet flow (Fig. 15b)

A period of relative sea level fall and significant evaporation is marked by the Amora Salt Member which is a 10 m thick halite interval dated at 420 ± 10 ka (Torfstein et al., 2009). No evidence is preserved to indicate that this salt member covered the growing salt wall, although it could admittedly have been subsequently removed via dissolution and erosion. However, we suggest that the arid conditions that led to evaporation and creation of the Amora Salt Member, also permitted a significant build-up of salt wall relief at about this time (Fig. 15b). We propose that this ultimately led to 'salt breakout', with at least part of the Lot Salt Member extruding towards the NE and flowing downslope towards the centre of the basin (Fig. 13b, Fig. 14 and Fig. 15b).

6.3. Stage 3 – continuation of salt sheet flow (Fig. 15c)

As salt continued to extrude and flow basinwards towards the NE, it caused the creation of a recumbent Bnot Lot fold within the salt wall (Fig. 11a, c and Fig. 15c). This fold can be traced for 5 km along strike, displays a hinge broadly parallel to the strike of the palaeoslope, and forms a 500 m wide inverted limb that we believe was driven and overturned by drag forces associated with lateral salt flow (Fig. 13b, Fig. 14 and Fig. 15c). The NW–SE orientation of the Bnot Lot fold hinge (Fig. 11b) is governed by the direction of salt flow down the regional palaeoslope, rather than the trend of the salt wall itself. The Bnot Lot shales forming the overturned limb within the salt wall eventually sheared towards the NE over the top of the Mearat Sedom Salt Member exposed along the NE margin of the salt wall. This resulted in the intense NE-verging folds and thrusts that are observed in both the caprock and overlying inverted Bnot Lot shales along the eastern flank of the salt wall (Fig. 7a). The underlying Mearat Sedom Salt Member was also inverted, with the overturned limb suffering extreme attenuation and even complete excision where overridden by the Bnot Lot shales (Fig. 7b).

6.4. Stage 4 – cessation of salt sheet flow (Fig. 15d)

Lateral salt sheet flow eventually ceased, perhaps brought about by either reduced rates of mobile salt supply and possible 'choking' of the feeder vent by clastics that locally comprise up to 25% of the evaporite sequence within the pinched area, coupled with increased dissolution of salt (Fig. 15d). Dissolution of salt (perhaps related to lake level rise) resulted in continued creation of caprock that is observed to rest directly on top of the overturned limb of the Bnot Lot fold (Fig. 12a–c). This relationship indicates that the Lot Salt Member, from which the caprock is derived, must have flowed directly over the top of the overturned shales. This caprock is however not significantly deformed, as it was created above the salt sheet, and therefore never had large amounts of salt shearing over the top of it.

6.5. Stage 5 – 'pinching' closed of the salt wall (Fig. 15e, f)

The central portion of the Sedom salt wall is marked by a swing in strike of its eastern margin from N–S trending to NW–SE orientations (Fig. 3). This results in a dramatic narrowing of the salt wall from 2000 m to just 800 m. We suggest that this narrowing, combined with a reduction in salt wall dips, late-stage SW verging folds (Fig. 10), and a 40° anticlockwise palaeomagnetic rotation (Weinberger et al., 1997) can be explained by the vent, that originally sourced the salt sheet extrusion, starting to close slightly as salt supply reduced (Fig. 14 and Fig. 15e, f).

6.6. Stage 6 – post salt wall subsidence (Fig. 15e, f)

The observation that sandstones and shales of the Upper Amora Member were deposited unconformably on top of the caprock overlying the Sedom salt wall (Zak, 1967), indicates that

the major phase of salt extrusion and dissolution to create this caprock must have ceased by this time (Fig. 15e, f). In addition, Zak (1967) reported fragments of caprock within the Upper Amora Member that sits unconformably on top of the Sedom salt wall. The age of the Upper Amora Member has been dated (at the Peratzim 2 borehole directly west of the salt wall) as ranging between 340 and 80 ka (Torfstein et al., 2009, p. 2620). Deposition of the Upper Amora Member directly over the Sedom salt wall indicates that it was buried at this time, with the thickest preservation of Upper Amora Member over the central pinched segment perhaps indicating the greatest subsidence over this former vent area (Fig. 3 and Fig. 15e, f).

6.7. Stage 7 – late extensional faulting (Fig. 15g)

Steep normal faults are developed around the flanks of the salt wall, and cut across the overturned Sedom Formation and overlying caprock along the eastern flank (Fig. 12d, e). This suggests a late stage top to the east extension of the overturned rocks potentially related to spreading (Fig. 15g). These structures cannot be early, pre-folding extensional faults overturned along with bedding, as discussed and depicted in the model of Graham et al. (2012, p. 605), as they have also cut the overlying caprock that formed after inversion of the sequence. The faults therefore represent a relatively late stage of post-folding east-directed extension and spreading.

7. Conclusions

The Sedom salt wall is one of the few places where halite and evaporites are exposed and accessible at the Earth's surface, thereby permitting direct observation of detailed structures associated with deformation of the salt and overburden. This leads us to a number of general conclusions.

a) Sediments forming the overburden to the salt are upturned for >300 m from the margin of the salt wall, with pronounced increases in bedding dips within 50 m of the margin, where the sediments ultimately have become entirely inverted and overridden by the salt. The amount of overburden upturn thus exponentially increases towards the salt, suggesting deformation of relatively weak overburden.
b) Folding and deformation within the evaporites is associated with sedimentary injections in the intervening clastic units and development of gypsum veins with vertical fibres indicating a 'jacking up' of the overlying sequence. This suggests that high fluid pressures have played a significant role in enhancing deformation within both clastics contained within the salt wall and adjacent overburden.
c) Clastic units within evaporites define the overall geometry of a km-scale recumbent fold developed within the salt wall, and show little internal deformation within the overturned limb of this fold. We suggest that folding of the overturned limb was facilitated by expulsion of salt from the hinge of the fold, together with high fluid pressures within the clastic units. Creation of recumbent folds is in direct response to gravity-driven flow of the adjacent salt sheet down the regional palaeoslope. The direction of salt flow is therefore governed by the orientation of slope rather than the trend of the pre-existing salt structure. It thus appears possible to generate entirely overturned sequences (i.e. inverted by 180°) that retain almost pristine sedimentary relationships within recumbent folds. This is the first direct observation and description of such overturned folds within exposed salt walls, although they have been interpreted from seismic sections (Jackson et al., 2014).
d) The multi-layer nature of the evaporites and associated clastic horizons has resulted in spectacular small scale boudinage of more competent marl and anhydrite horizons within the salt wall. On a larger scale, folding is interpreted to form during both the lateral outward flow of salt, and subsequent pinching closed of the former vent.
e) Dramatic thinning (×20) of salt members from ~380 m to < 20 m is achieved along just 200 m of strike length within the salt wall. Such profound changes in thickness are associated with the salt having passed onto the overturned limb of the fold, and are consistent with extreme attenuation and potential lateral extrusion of salt into a sheet.
f) The margins of the salt wall are typically marked by steep, outward-dipping normal faults which are sub-parallel to bedding within the salt wall and overburden. However, where the salt flank and adjacent overburden have become entirely overturned, such as associated with lateral salt sheet flow, then extensional faults have cut through this inverted sequence at high angles to bedding. This failure of the margin allows the salt wall to continue rising in a 'piston-like' manner even where bedding in the overburden and within the salt wall are not favourably orientated.

In addition to the broad conclusions listed above, a general evolutionary model has been developed that links the formation of recumbent folds within the Sedom salt wall with lateral flow of salt. The slope parallel orientation of the recumbent fold hinge, the NE-directed overturning of the recumbent limb, the subsequent development of NE-verging folds and thrusts and the overturning of overburden along the eastern margin all suggest that salt breakout and associated salt sheet flow was directed basinwards towards the NE. Salt breakout is thought to occur at about 420 ka, and was followed by pinching closed of the former vent resulting in the pronounced hour-glass map pattern. The salt wall was subsequently buried by the Upper Amora Member that ranges in age between 340 and 80 ka (Torfstein et al., 2009). The salt wall continued to grow, as demonstrated by the uplift of the top Lisan Formation dated at 15.5 ka to 75 m above its regional elevation, indicating mean uplift rates of ~5 mm/year, while InSAR reveals modern uplift in the range of 5.5–8 mm/year (Weinberger et al., 2006b).

Acknowledgements

GIA is grateful for funding from the Carnegie Trust for the Universities of Scotland that enabled fieldwork for this project. RW was supported by the Israel Science Foundation (ISF grant No. 1245/11). SM was supported by the Israel Science Foundation (ISF grant No. 1736/11). We thank Ian Davison and Chris Talbot for their careful and constructive reviews of the manuscript.

References

Aftabi, P., Roustaie, M., Alsop, G.I., Talbot, C.J., 2010. InSAR mapping and modelling of an active Iranian salt extrusion. J. Geol. Soc. Lond. 167, 155–170.
Agnon, A., Weinberger, R., Zak, I., Sneh, A., 2006. Geological Map of Israel. Sheet 20-I, II Sedom, Scale 1:50,000. Israel Geological Survey, Jerusalem.
Alsop, G.I., 1996. Physical modelling of fold and fracture geometries associated with salt diapirism. In: Alsop, G.I., Blundell, D.J., Davison, I. (Eds.), Salt Tectonics, Geological Society, London, Special Publications, vol. 100, pp. 227–241.
Alsop, G.I., Brown, J.P., Davison, I., Gibling, M.R., 2000. The geometry of drag zones adjacent to salt diapirs. J. Geol. Soc. Lond. 157, 1019–1029.
Alsop, G.I., Marco, S., 2011. Soft-sediment deformation within seismogenic slumps of the Dead Sea Basin. J. Struct. Geol. 33, 433–457.
Alsop, G.I., Marco, S., 2012. A large-scale radial pattern of seismogenic slumping towards the Dead Sea Basin. J. Geol. Soc. 169, 99–110.

Alsop, G.I., Marco, S., 2013. Seismogenic slump folds formed by gravity-driven tectonics down a negligible subaqueous slope. Tectonophysics 605, 48–69.
Alsop, G.I., Marco, S., 2014. Fold and fabric relationships in temporally and spatially evolving slump systems: a multi-cell flow model. J. Struct. Geol. 63, 27–49.
Al-Zoubi, A., ten Brink, U.S., 2001. Salt diapirs in the Dead Sea basin and their relationship to quaternary extensional tectonics. Mar. Petroleum Geol. 18, 779–797. http://dx.doi.org/10.1016/S0264-8172(01)00031-9.
Albertz, M., Ings, S.J., 2012. Some consequences of mechanical stratification in basin-scale numerical models of passive-margin salt tectonics. In: Alsop, G.I., Archer, S.G., Hartley, A.J., Grant, N.T., Hodgkinson, R. (Eds.), Salt Tectonics, Sediments and Prospectivity, Geological Society, London, Special Publications, vol. 363, pp. 303–330.
Archer, S.G., Alsop, G.I., Hartley, A.J., Grant, N.T., Hodgkinson, R., 2012. Salt tectonics, sediments and hydrocarbon prospectivity. In: Alsop, G.I., Archer, S.G., Hartley, A.J., Grant, N.T., Hodgkinson, R. (Eds.), Salt Tectonics, Sediments and Prospectivity, Geological Society, London, Special Publications, vol. 363, pp. 1–6. http://dx.doi.org/10.1144/SP363.1.
Barnhart, W.D., Lohman, R.B., 2012. Regional trends in active diapirism revealed by mountain range-scale InSAR time series. Geophys. Res. Lett. 39, 1.08309.
Burliga, S., 2014. Heterogeneity of folding in Zechstein (Upper Permian) salt deposits in the Klowdawa salt structure, central Poland. Geol. Q. 58, 565–576.
Butler, R.W.H., 1992. Structural evolution of the western Chartreuse fold and thrust system, NW French Sub-alpine chains. In: McClay, K.R. (Ed.), Thrust Tectonics. Chapman & Hall, London, pp. 287–298.
Butler, R.W.H., Coward, M.P., Harwood, G.M., Knipe, R.J., 1987. Salt control on thrust geometry, structural style and gravitational collapse along the Himalayan Mountain Front in the Salt Range of Northern Pakistan. In: Lerche, I., O'Brien, J.J. (Eds.), Dynamical Geology of Salt and Related Structures. Academic Press, pp. 339–418.
Cartwright, J., Jackson, M., Dooley, T., Higgins, S., 2012. Strain partitioning in gravity-driven shortening of a thick, multilayered evaporite sequence. In: Alsop, G.I., Archer, S.G., Hartley, A.J., Grant, N.T., Hodgkinson, R. (Eds.), Salt Tectonics, Sediments and Prospectivity, Geological Society, London, Special Publications, vol. 363, pp. 449–470.
Davison, I., Bosence, D., Alsop, G.I., Al-Aawah, M.H., 1996. Deformation and sedimentation around active Miocene salt diapirs on the Tihama Plain, northwest Yemen. In: Alsop, G.I., Blundell, D.J., Davison, I. (Eds.), Salt Tectonics, Geological Society, London, Special Publications, vol. 100, pp. 23–39.
Dooley, T.P., Jackson, M.P.A., Hudec, M.R., 2014. Breakout of squeezed stocks: dispersal of roof fragments, source of extrusive salt and interaction with regional thrust faults. Basin Res. 26, 1–23. http://dx.doi.org/10.1111/bre.12056.
Farkash, L., Litman, H.L., Bloch, M.R., 1951. The formation of "salt tables" in natural and artificial solar pans. Res. Counc. Israel Bull. 1, 36–39.
Fiduk, J.C., Rowan, M.G., 2012. Analysis of folding and deformation within layered evaporites in Blocks BM-S-8 & -9, Santos Basin, Brazil. In: Alsop, G.I., Archer, S.G., Hartley, A.J., Grant, N.T., Hodgkinson, R. (Eds.), Salt Tectonics, Sediments and Prospectivity, Geological Society, London, Special Publications, vol. 363, pp. 471–487.
Frumkin, A., 1996a. Uplift rate relative to base-levels of a salt diapir (Dead Sea basin, Israel) as indicated by cave levels. In: Alsop, G.I., Blundell, D.J., Davidson, I. (Eds.), Salt Tectonics, Geological Society of America Special Publication, vol. 100, pp. 41–47.
Frumkin, A., 1996b. Determining the exposure age of a karst landscape. Quat. Res. 46, 99–106. http://dx.doi.org/10.1006/qres.1996.0050.
Frumkin, A., 1996c. Structure of northern Mount Sedom salt diapir (Israel) from cave evidence and surface morphology. Israel J. Earth Sci. 45, 73–80.
Frumkin, A., 2009. Formation and dating of a salt pillar in Mount Sedom diapir, Israel. Geol. Soc. Am. Bull. 121, 286–293. http://dx.doi.org/10.1130/B26376.1.
Fuchs, L., Koyi, H., Schmeling, H., 2014. Numerical modeling on progressive internal deformation in down-built diapirs. Tectonophysics 632, 111–122.
Gardosh, M., Kashai, E., Salhov, S., Shulman, H., Tannenbaum, E., 1997. Hydrocarbon exploration in the southern Dead Sea area. In: Niemi, T.M., Ben-Avraham, Z., Gat, J.R. (Eds.), The Dead Sea: the Lake and its Setting. Oxford University Press, Oxford, pp. 57–72.
Garfunkel, Z., 1981. Internal structure of the Dead Sea leaky transform (rift) in relation to plate kinematics. Tectonophysics 80, 81–108. http://dx.doi.org/10.1016/0040-1951(81)90143-8.
Ghosh, S.K., 1993. Structural Geology: Fundamentals and Modern Developments. Pergamon press, p. 598.
Giles, K.A., Rowan, M.G., 2012. Concepts in halokinetic-sequence deformation and stratigraphy. In: Alsop, G.I., Archer, S.G., Hartley, A.J., Grant, N.T., Hodgkinson, R. (Eds.), Salt Tectonics, Sediments and Prospectivity, Geological Society, London, Special Publications, vol. 363, pp. 7–31.
Graham, R., Jackson, M., Pilcher, R., Kilsdonk, B., 2012. Allochthonous salt in the sub-Alpine fold-thrust belt in Haute Provence, France. In: Alsop, G.I., Archer, S.G., Hartley, A.J., Grant, N.T., Hodgkinson, R. (Eds.), Salt Tectonics, Sediments and Prospectivity, Geological Society, London, Special Publications, vol. 363, pp. 595–615.
Haase-Schramm, A., Goldstein, S.L., Stein, M., 2004. U–Th dating of Lake Lisan aragonite (late Pleistocene Dead Sea) and implications for glacial East Mediterranean climate change. Geochimica Cosmochimica Acta 68, 985–1005.
Harrison, J.C., Jackson, M.P.A., 2013. Exposed evaporite diapirs and minibasins above a canopy in central Sverdrup Basin, Axel Heiberg Island, Arctic Canada. Basin Res. 25, 1–30. http://dx.doi.org/10.1111/bre.12037.
Hudec, M.R., Jackson, M.P.A., 2006. Advance of allochthonous salt sheets in passive margins and orogens. Am. Assoc. Petroleum Geologists Bull. 90, 1535–1564.
Hudec, M.R., Jackson, M.P.A., 2011. The Salt Mine: a Digital Atlas of Salt Tectonics. In: Bureau of Economic Geology, Udden Book Series No. 5; American Association of Petroleum Geology Memoir, vol. 99. The University of Texas at Austin, p. 305.
Jackson, C.A.-L., Jackson, M.P.A., Hudec, M.R., Rodriguez, C., 2014. Internal structure, kinematics, and growth of a salt wall: insights from 3-D seismic data. Geology 42, 307–310. http://dx.doi.org/10.1130/G34865.1.
Jackson, M.P.A., Talbot, C.J., 1989. Anatomy of mushroom-shaped diapirs. J. Struct. Geol. 11, 211–230.
Joffe, S., Garfunkel, Z., 1987. Plate kinematics of the circum Red Sea – a re-evaluation. Tectonophysics 141, 5–22. http://dx.doi.org/10.1016/0040-1951(87)90171-5.
Levi, T., Weinberger, R., Eyal, Y., Lyakhovsky, V., Heifetz, E., 2008. Velocities and driving pressures of clay-rich sediments injected into clastic dikes during earthquakes. Geophys. J. Int. 175, 1095–1107.
Masrouhi, A., Koyi, H.A., 2012. Submarine 'salt glacier' of Northern Tunisia, a case of Triassic salt mobility in North African Cretaceous passive margin. In: Alsop, G.I., Archer, S.G., Hartley, A.J., Grant, N.T., Hodgkinson, R. (Eds.), Salt Tectonics, Sediments and Prospectivity, Geological Society, London, Special Publications, vol. 363, pp. 579–593.
Masrouhi, A., Bellier, O., Youssef, M.B., Koyi, H., 2014. Submarine allochthonous salt sheets: gravity-driven deformation of North African Cretaceous passive margin in Tunisia – Bled Dogra case study and nearby salt structures. J. Afr. Earth Sci. 97, 125–142.
Matmon, A., Fink, D., Davis, M., Niedermann, S., Rood, D., Frumkin, A., 2014. Unraveling rift margin evolution and escarpment development ages along the Dead Sea fault using cosmogenic burial ages. Quat. Res. 82, 281–295.
Platt, J.P., 1982. Emplacement of a fold-nappe, Betic Orogen, southern Spain. Geology 10, 97–102.
Poprawski, Y., Basile, C., Agirrezabala, L., Jaillard, E., Gaudin, M., Jacquin, T., 2014. Sedimentary and structural record of the Albian growth of the Baikio diapir (the Basque Country, northern Spain). Basin Res. http://dx.doi.org/10.1111/bre.12062.
Price, N.J., Cosgrove, J.W., 1990. Analysis of Geological Structures. Cambridge University Press.
Quintà, A., Tavani, S., Roca, E., 2012. Fracture pattern analysis as a tool for constraining the interaction between regional and diapir-related stress fields: Poza de la Sal Diapir (Basque Pyrenees, Spain). In: Alsop, G.I., Archer, S.G., Hartley, A.J., Grant, N.T., Hodgkinson, R. (Eds.), Salt Tectonics, Sediments and Prospectivity, Geological Society, London, Special Publications, vol. 363, pp. 521–532.
Quirk, D.G., Pilcher, R.S., 2012. Flip-flop salt tectonics. In: Alsop, G.I., Archer, S.G., Hartley, A.J., Grant, N.T., Hodgkinson, R. (Eds.), Salt Tectonics, Sediments and Prospectivity, Geological Society, London, Special Publications, vol. 363, pp. 245–264.
Ramsay, J.G., 1967. Folding and Fractruring of Rocks. McGraw-Hill, New York.
Richter-Bernburg, G., 1980. Salt tectonics, interior structures of salt bodies. Bull. Cent. Rech. Explor.-Prod. Elf Aquitane 4, 373–393.
Ringenbach, J.-C., Salel, J.-F., Kergaravat, C., Ribes, C., Bonnel, C., Callot, J.-P., 2013. Salt tectonics in the Sivas Basin, Turkey: outstanding seismic analogues from outcrops. First Break 31, 93–101.
Rowan, M.G., Vendeville, B.C., 2006. Foldbelts with early salt withdrawal and diapirism: Physical model and examples from the northern Gulf of Mexico and ther Flinders Ranges, Australia. Mar. Petrol. Geol. 23, 871–891.
Rowan, M.G., Lawton, T.F., Giles, K.A., 2012. Anatomy of an exposed vertical salt weld and flanking strata, La Popa Basin, Mexico. In: Alsop, G.I., Archer, S.G., Hartley, A.J., Grant, N.T., Hodgkinson, R. (Eds.), Salt Tectonics, Sediments and Prospectivity, Geological Society, London, Special Publications, vol. 363, pp. 33–57.
Saura, E., Verges, J., Martin-Martin, J.D., Messager, G., Moragas, M., Razin, P., Grelaud, C., Joussiaume, R., Malaval, M., Homke, S., Hunt, D.W., 2014. Syn- to post-rift diapirism and minibasins of the Central High Atlas (Morocco): the changing face of a mountain belt. J. Geol. Soc. Lond. 171, 97–105. http://dx.doi.org/10.1144/jgs2013-079.
Sneh, A., Weinberger, R., 2014. Major Structures of Israel and Environs, Scale 1: 50,000. Israel Geological Survey, Jerusalem.
Storti, F., Balsamo, F., Cappanero, F., Tosi, G., 2011. Sub-seismic scale fracture pattern and in situ permeability data in the chalk atop of the Krempe salt ridge at Lagerdorf, NW Germany: inferences on synfolding stress field evolution and its impact on fracture connectivity. Mar. Petrol. Geol. 7, 1315–1332.
Strozyk, F., Van Gent, H., Urai, J.L., Kukla, P.A., 2012. 3D seismic study of complex intra-salt deformation: an example from the Upper Permian Zechstein 3 stringer, western Dutch offshore. In: Alsop, G.I., Archer, S.G., Hartley, A.J., Grant, N.T., Hodgkinson, R. (Eds.), Salt Tectonics, Sediments and Prospectivity, Geological Society, London, Special Publications, vol. 363, pp. 489–501.
Talbot, C.J., 1979. Fold trains in a glacier of salt in southern Iran. J. Struct. Geol. 1, 5–18.
Talbot, C.J., 1998. Extrusions of Hormuz salt in Iran. In: Blundell, D.J., Scott, A.C. (Eds.), Lyell: the Past Is the Key to the Present, Geological Society, London, Special Publications, vol. 143, pp. 315–334.
Talbot, C.J., Jackson, M.P.A., 1987. Internal kinematics of salt diapirs. AAPG Bull. 71, 1068–1093.
Torfstein, A., Haase-Schramm, A., Waldmann, N., Kolodny, Y., Stein, M., 2009. U-series and oxygen isotope chronology of the mid-Pleistocene Lake Amora (Dead Sea Basin). Geochimica Cosmochimica Acta 73, 2603–2630.

Vargas-Meleza, L., Healy, D., Alsop, G.I., Timms, N.E., 2015. Exploring the relative contribution of mineralogy ad CPO to the seismic velocity anisotropy of evaporates. J. Struct. Geol. 70, 39–55.

Weinberger, R., Agnon, A., Ron, H., 1997. Paleomagnetic reconstruction of a diapir emplacement: a case study from sedom diapir, the dead sea rift. J. Geophys. Res. 102, 5173–5192.

Weinberger, R., Begin, Z.B., Waldmann, N., Gardosh, M., Baer, G., Frumkin, A., Wdowinski, S., 2006a. Quaternary rise of the Sedom diapir, Dead Sea basin. In: Enzel, Y., Agnon, A., Stein, M. (Eds.), New Frontiers in Dead Sea Paleoenvironmental Research, Geol. Soc. Am. Special Paper, vol. 401, pp. 33–51. http://dx.doi.org/10.1130/2006.2401(03).

Weinberger, R., Lyakhovsky, V., Baer, G., Begin, Z.B., 2006b. Mechanical modeling and InSAR measurements of Mount Sedom uplift, Dead Sea Basin: implications for rock-salt properties and diapir emplacement mechanism. Geochem. Geophys. Geosyst. 7, Q05014. http://dx.doi.org/10.1029/2005GC001185.

Weinberger, R., Bar-Matthews, M., Levi, T., Begin, Z.B., 2007. Late-Pleistocene rise of the Sedom diapir on the backdrop of water-level fluctuations of Lake Lisan, Dead Sea basin. Quat. Int. 175, 53–61. http://dx.doi.org/10.1016/j.quaint.2007.03.007.

Zak, I., 1967. The Geology of Mount Sedom. Ph.D. thesis. The Hebrew University of Jerusalem, p. 208 (in Hebrew with an English abstract).

Zak, I., Bentor, Y.K., 1972. Some new data on the salt deposits of the Dead Sea area, Israel. In: Geology of Saline Deposits. Proceedings of the Hannover Symposium, 1968: Earth Sciences, vol. 7. UNESCO, Paris, pp. 137–146.

Zak, I., Freund, R., 1980. Strain measurements in eastern marginal shear zone of Mount Sedom salt diapir, Israel. AAPG Bull. 64, 568–581.

Zak, I., Karcz, I., Key, C.A., 1968. Significance of some sedimentary structures from Mount Sedom. Israel J. Earth Sci. 17, 1–8.